Journal of Molecular Graphics and Modelling 27 (2009) 951–968

Contents lists available at ScienceDirect

Journal of Molecular Graphics and Modelling

journal homepage: www.elsevier.com/locate/JMGM

Atomistic visualization: Space–time multiresolution integration of data analysis and rendering

Dipesh Bhattarai [a], Bijaya B. Karki [a,b,*]

[a] Department of Computer Science, Louisiana State University, Baton Rouge, Louisiana 70803, USA
[b] Department of Geology and Geophysics, Louisiana State University, Baton Rouge, Louisiana 70803, USA

A R T I C L E I N F O

Article history:
Received 9 December 2008
Received in revised form 30 January 2009
Accepted 6 February 2009
Available online 20 February 2009

Keywords:
Scientific visualization
Atomistic visualization
Molecular dynamics simulations
Structural properties
Dynamical properties
Silicate liquids

A B S T R A C T

Time-varying three-dimensional scattered data representing snapshots of atomic configurations produced by molecular dynamics simulations are not illuminating by themselves; gaining insight into them poses a tremendous challenge. In order to take the advantage of maximal information offered by these simulations, we have proposed an efficient scheme, which integrates various analysis and rendering tasks together in order to support interactive visualization of the data at space–time multiresolution. Additional data produced by various analytical techniques on the fly represent the atomic system under consideration at diverse length- (e.g., nearest neighbor, next-nearest neighbor or beyond) and time- (e.g., instantaneous, finite intervals or overall averages) scales. In particular, the radial distribution functions, coordination environments, clusters and rings are computed and visualized to understand the structural behavior whereas a variety of displacement data and covariance matrices are explored to understand the dynamical behavior. While the spatial distributions of atoms need to be reproduced correctly during rendering, we take the advantage of high flexibility in rendering other attributes because of the lack of their direct physical relevance. A combination of different techniques including animation, color maps, pathlines, different types of glyphs, and graphics hardware accelerated approach is exploited to render the original and extracted data. First-principles molecular dynamics simulation data for liquid systems are used to justify the effectiveness and usefulness of the proposed scheme.

1. Introduction

Atomistic (molecular) visualization is one of the most widely studied scientific applications of visualization. Time-dependent three-dimensional scattered data from molecular dynamics simulations represent snapshots of atomic configurations and they are known to be rich in the structural and dynamical information. To gain insight into such correlated dynamical data, visualization has previously been exploited in different ways depending on the nature of the atomic systems studied. For crystalline solids in which the atoms have well-defined positions, the most of the existing visualization methods are directly applicable. On the other hand, disordered systems such as liquids and amorphous solids show weak or no long-range order. Even the short-range (local) order is temporal to a great extent and transient fluctuations are expected to occur. While many physical properties at macroscopic scale are often obtained as statistical averages, understanding them at microscopic (atomic) scale requires a detailed examination of individual snapshots. Visualization in usual sense tries to render a given dataset using various glyphs representing the atoms and bonds, or other structures already existing in the dataset. A lot of work has been previously done in this context. Some common examples include Molscript [1], VMD [2], XcrysDen [3], Atomeye [4], Atomsviewer [5,6], CrystalMaker (http://www.crystalmaker.com), amiraMol (http://www.amira-vis.com/mol), Aviz, gOpenMol, VASP DataViewer, PyMD, etc. In general, the existing visualization systems share many features (see a review by Li [7]):

- A wide variety of representation (rendering and coloring) modes such as balls, points and lines, balls and sticks, space-fill and polyhedra
- Real-time manipulations such as rotation, translation, scaling and selection
- Measurement of distances, angles, and dihedrals
- Crystalline properties (e.g., switching between primitive and conventional cell settings, displaying the Wigner–Seitz cell and Brillouin-zone)

* Corresponding author.
E-mail address: karki@csc.lsu.edu (B.B. Karki).

1093-3263/$ – see front matter © 2009 Elsevier Inc. All rights reserved.
doi:10.1016/j.jmgm.2009.02.005

- Animations (particularly, for MD simulation trajectories) imported either from files or from a direct connection to a running MD simulation
- Support for a variety of database files from a variety of simulation sources.

Offline analyses of the data are used to further understand the atomic position time series [8–10]. How visualization can help in exploring the results derived from such analyses has yet to be addressed in a more complete way. To the best of our knowledge, all previous visualization schemes [7] have a little, if not at all, capability to analyze and visualize the atomic data at multiple length- and time-scales. Our scheme primarily differs from previous schemes in that we integrate data analysis and rendering tasks to support interactive atomistic visualization at space–time multiresolution. We have previously reported some preliminary ideas and results [11–13]. In particular, the analyses produce various data on the fly that represent a given atomic system at diverse length- (e.g., nearest neighbors or second-nearest neighbors or beyond) and time- (instantaneous or finite intervals or overall averages) scales. The information is thus processed at varying levels of details. Instead of directly rendering the input positional data, additional data that usually have to be extracted by offline analyses are extracted and rendered on the fly. The extracted data are rendered as soon as they are generated to support an interactive visualization. Depending upon the nature of the materials problem, the information that has to be extracted from the simulation data may vary considerably so that one single scheme may not be suitable for the complete information extraction. It warrants that a combined analysis and visualization scheme be developed accordingly to meet domain specific needs. For instance, our main focus here is on visualization of the outputs from first-principles molecular dynamics (FPMD) simulations (within the framework of quantum mechanics) of defective and disordered systems, e.g., [14]. Such simulations are known to be highly accurate so it is important that we exploit the richness of the information contained in such simulations.

Our scheme is aimed at exploring both the structural and dynamical aspects of a position-time series. First, to gain insight into local structure or short- to mid-range order in a given material system, we compute and visualize coordination environments, clusters and rings. This requires knowledge of the radial distribution function, which determines the average density of atoms at a distance from a specified atom. For instance, the atoms that can be found under the first peak of the radial distribution function are usually considered to determine coordination environment, which tells us how atoms are arranged in the immediate neighborhood of each atom. Clusters, which represent a group of atoms formed based on similarity between neighbors are useful in identifying atoms in particular environment such as fcc, hcp, bcc or icosahedral [15]. Rings formed by the atoms can help us describe the topology of the network forming systems like silica [9,16]. Second, dynamical behavior tells us how and to what extent the constituent atoms move. Normally, atomic positions are rendered as a function of time to give a feeling of dynamics. However, we extract and visualize a variety of atomic displacement data. For instance, it's interesting to quantify and visualize the extent of a constituent atom's drift from some reference position (e.g., initial or mean position) or during the whole simulation period. We use the principal component analysis to understand the diffusive nature of the atoms and anisotropy of their movement.

The rest of the paper is organized as follows. We first describe the simulation data visualized using our scheme. Different analytical and rendering techniques used to visualize the structural and dynamical properties of the simulated systems at multi-levels of details are then presented. This is followed by the design and implementation of the atomistic visualization system. Finally, we present conclusions and important future directions.

2. Simulation data

In recent years, studies of complex materials systems like liquids and defect-containing solids using first-principles molecular dynamics simulation methods have become widespread. Unlike perfect crystals in which the symmetry constrains the simulation size (often unit cells with periodic boundary conditions are used) as well as the atomic configuration (a few free positional parameters need to be considered explicitly), liquids and defective systems require much larger atomic systems and the crystal symmetry is violated partially or completely. For example, MgO in its conventional simple cubic structure requires only 8 atoms whose positions are fixed by the cubic symmetry. A liquid MgO uses as many as 216 atoms [17] so that a discrete set of 648 (positional) degrees of freedom need to be explicitly taken into account. The atomic positions of a liquid phase are strongly correlated but without any long-range order. Visualization of the data at different resolutions of length and time allows us to gain insight into the complex structural and dynamical nature of the liquid state.

In first-principles molecular dynamics or more generally, in any molecular dynamics simulation, a system is initially defined by a group of properties that represent atomic positions, atomic types, and constraints that have to be satisfied [8]. Let A be the collection of $\{R, S, C\}$ describing the system. Here, $R = \{r_i \in X \subset \Re 3\}$ (X demarcates the simulation box) is the set of the atomic positions in the system, which can be considered as discrete degrees of freedom. $S = \{s \in \text{types}\}$ is the set of the atomic types (for instance, Mg, Si and O atoms for a silicate liquid). C is the set of constraints that has to be satisfied by the system. For example, in the FPMD simulation based on canonical NVT ensemble, the number of atoms in the supercell (N), the volume (V), and the temperature (T) are fixed. As the simulation progresses, a new system configuration is generated. Collection of A's over a given simulation time duration describes the system dynamics, i.e., $D = \{A_t | 0 \leq t \leq \mathfrak{T}\}$. In essence, FPMD computes the trajectories, i.e., positions $\{r_i \mid i = 1, \ldots, N\}$ as a function of time t, of all the atoms by numerically integrating the Newton's equations of motion:

$$m_i \frac{d^2 r_i}{dt^2} = F_i \qquad (1)$$

where m_i is the mass of atom i and $F_i = \sum_{i \neq j} f_{ij}$ is the force on atom i due to all the other atoms. In FPMD, these interatomic forces are derived from a fully self-consistent solution of the electronic structure problem within density functional theory [18]. Such quantum mechanical method is computationally more intensive than the methods based on simplified potential models.

The position-time series data used in this study were generated from parallel FPMD simulations of liquids. Our analysis and visualization primarily deals with the simulated silicate liquid containing 10 wt% water [14]. The simulation supercell consists of 168 atoms, i.e., 24 $MgSiO_3$ units and 16 water molecules. The simulation runs range from a few thousands steps to a couple of hundred thousands of steps with 0.5 fs time step. The output results reported in the paper refer to this hydrous silicate system unless other systems (MgO [17] or silica liquid [19]) are explicitly mentioned. It is important to note that FPMD simulations also produce data related to electronic structures (e.g., [17]) such as charge density distribution and wave functions, however, their visualization is beyond the scope of the present work.

3. Visualizing structural properties

3.1. Radial distribution function

The radial distribution function (RDF) is the simplest but most commonly used form of many distribution functions that can be defined for the atomic positions in a dynamical system [8]. It is also called the pair correlation function. The function gives the probability of finding a pair of atoms a distance r apart, relative to the probability expected for a completely random distribution at the same density. As such, it represents the average radial packing of the atoms and is used to concisely characterize the structure of complex systems like liquids and colloidal suspensions. In such systems, the particles are in a constant motion and a single snapshot of the system shows only the instantaneous disorder. The structure has meaning, in general, in an average sense and RDF is often considered an effective way of describing such average structure. Another advantage is that it can be measured experimentally using neutron and X-rays diffraction techniques allowing us to compare simulations with experiments. Finally, in the case of the pair-wise potential function, thermodynamic quantities, particularly, the energy and pressure can be expressed directly in terms of RDF.

RDF of a crystalline system in which the constituent atoms wander about their equilibrium positions in a lattice shows sharp peaks at fixed distances and is zero everywhere else. On the other hand, RDF of a disordered system like a liquid shows different patterns (Fig. 1). After some initial distance, it picks a non-zero value up and sharply increases to reach a peak value, which may not be as well defined as it is in the case of crystal. As the radial distance increases, RDF decreases to reach some minimum value (often larger than zero) and thereafter may show another shallow peak before it starts to fluctuate around the unity eventually converging to the unity at larger distances. The atoms too far from each other are statistically uncorrelated so there is no long-range order. For a system with more than one type of atoms, we have to differentiate between the function that describes radial distribution of the particles irrespective of their types (atomic species), called total RDF and those that describe radial distribution of the atoms of certain type around atoms of another type, called partial RDF. Taking atomic species into consideration enables a detail analysis of a multi-species system and is useful when distribution of one atomic species around another atomic species is important. For example, in silicate phases, distributions of oxygen atoms around magnesium or silicon atoms are of special interest. The radial distribution function for atomic pair of species α and β is defined by

$$g_{\alpha\beta}(r) = \frac{1}{4\pi\rho_\beta r^2}\left[\frac{\Delta N_\beta(r)}{\Delta r}\right] \tag{2}$$

where $\rho_\beta = N_\beta/V$ is the number density of species β. For a finite-size supercell used in the simulation, the RDF computation has to take the imposed periodic boundary conditions into account.

We use the binning method for the RDF computation. This involves constructing a series of concentric spheres set at a fixed distance (Δr) apart around each atom of species α in the system and counting the atoms of species β in each shell. The total number of species β in the shell of radius r and width Δr is defined as:

$$\Delta N_\beta(r) = \sum_{i=1}^{N_\alpha}\sum_{\substack{j=1\\ j\neq i}}^{N_\beta} I(r \le d(p_i, p_j) \le r + \Delta r) \tag{3}$$

Here, $d(p_i,p_j)$ is a distance function that computes Euclidean distance between two points, and the indicator function for a predicate p, $I(p)$, is 1 if p is true and 0 otherwise. There are N_α and N_β particles of these species. The calculated number of atoms in the shell needs to be normalized by the number that would be observed if the atoms were uncorrelated. A chosen maximum distance $d_{\max}$ up to which we want to compute RDF is divided into a number of bins, n_{bins} so that $\Delta r = d_{\max}/n_{\text{bins}}$. Note that these bins correspond to the spherical shells of width Δr of increasing radius. The atom pairs whose inter-atomic distances fall within individual bins are counted. All the atoms at a distance $0 < r \le \Delta r$ are put in bin_0, atoms at a distance $\Delta r < r \le 2\Delta r$ are put in bin_1. In general, atoms at a distance $i^*\Delta r < r \le (i+1)^*\Delta r$ are put in bin_i. Thus computed RDF is for an atomic configuration at a particular time instant. An instantaneous RDF fluctuates too rapidly without conveying much useful information. Also as the system is assumed to be ergodic, time averaged distribution is supposed to represent a meaningful distribution. We perform an average over an extended simulation period:

$$\Delta\hat{N}_\beta(r) = \frac{\int_0^\tau \Delta N_\beta^t(r)\,\mathrm{d}t}{\int_0^\tau \mathrm{d}t} \tag{4}$$

Here, $\Delta N_\beta^t(r)$ is time-indexed version of $\Delta N_\beta(r)$ and its time average $\Delta\hat{N}_\beta(r)$ is used in the calculation of RDF. Being a probabilistic function, a physically significant RDF requires the system be simulated for a sufficiently long time.

There are several ways for speeding up the RDF computation. First, the atomic positions are time-correlated and from one time step to another time step they do not change substantially. This allows step skipping during the RDF computation without significantly affecting the accuracy. Second, unlike crystalline solids in which the structure is periodic and well defined, in disordered systems RDF shows well-defined peaks only at relatively short distances (Fig. 1). This suggests that we can choose a small value for $d_{\max}$ such that only the first and second peaks are covered. Third, we can increase the size of bin or equivalently decrease the number of bins. The curves are then smoothed if needed. Smoothing is, in general, useful to precisely compute the positions of the peaks and minima since the calculated RDF is subject to statistical noise, which can be relatively large in some cases due to poor sampling. Smoothing is achieved by a local fitting in r. Finally, one can perform partial

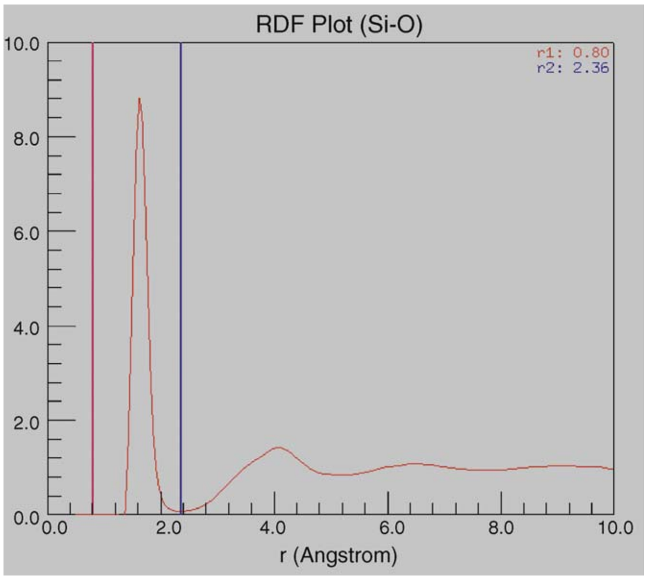

Fig. 1. Si–O radial distribution function for the hydrous silicate liquid. The vertical lines (red and blue) are used to mark the critical distances.

RDF computation selectively since often a small subset of partial RDFs is of particular importance and frequent use.

RDF can be considered as a starting point for a detailed structural analysis of disordered systems. The presence of one or more peaks at relatively short distances means that the system exhibits a short- to mid-range order. To fully explore such structures, information on critical distances indicating the positions of peaks and minima such as the distance to the first minimum (r_{min}) is needed. Also, a cutoff window of arbitrary width can be selected to further examine structural correlation. For instance, one can calculate the bond length as a weighted average of all distances covered by the first peak by integrating $g_{\alpha\beta}(r)$ up to r_{min}. Similarly, critical distances are used in computing bond angles, coordination, clusters, etc. The RDF plot allows the user to interactively pick up and adjust as necessary the critical distances or window widths used by subsequent analysis. Moreover, the user can vary in real time the range of steps, the size of skipping, the number of bins, the maximum distance, and atomic species to achieve desired performance. A square matrix plot is used to simultaneously render the complete set of partial RDFs for a multi-component system (Fig. 2). However, we can also render only a subset; a row plot rendering RDFs of all species about one selected species whereas a column plot rendering RDFs of a given species about all species. Finally, a single plot renders only one RDF corresponding to a selected pair of species exploiting a full display space so that its details can be better explored. In this mode, RDF can be decomposed into multiple components by treating structurally unequivalent atoms of the same species differently (Fig. 3).

3.2. Coordination environment

Atomic coordination, which is an important property used for characterizing the local structure, can be calculated for a given species α with respect to another species β as:

$$C_{\alpha\beta} = 4\pi\rho_\beta \int_{r_1}^{r_2} r^2 g_{\alpha\beta}(r)dr \tag{5}$$

Normally, we choose $r_1 = 0$ and $r_2 = r_{\text{min}}^{\alpha\beta}$, a distance window which covers the first peak in RDF (Fig. 1). In this case, the Eq. (5) gives the average number of atoms of species β that lie within spherical regions around atoms of species α and of radius $r_C = r_{\text{min}}^{\alpha\beta}$, called the coordination distance. $C_{\alpha\beta}$ represents the nearest neighbor coordination number and corresponds to the first coordination shell. The atomic distances, which fall between $r_1 = r_{\text{min}}^{\alpha\beta}$ and r_2 = the minimum after the second peak, determine the second coordination shell. Since the second peak is poorly defined generally in disordered system, our coordination analysis only deals with the first shell. Coordination represents the structure in a

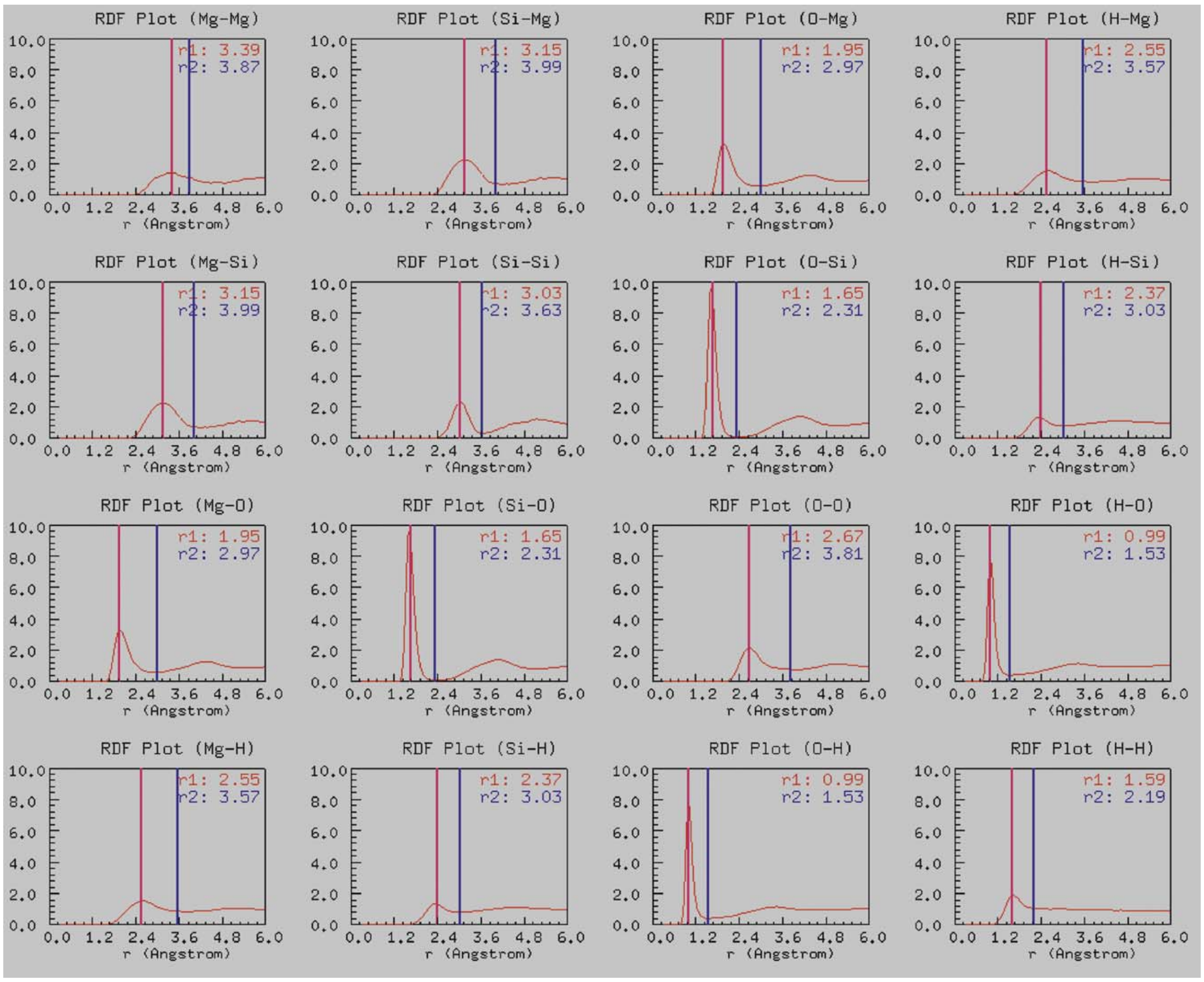

Fig. 2. RDF matrix (symmetric) plot rendering all partial radial distribution functions (considering both like-atom pairs and unlike-atom pairs) for the hydrous silicate liquid. The vertical lines mark the critical distances, the first peak position (red line) and the minimum position (blue line).

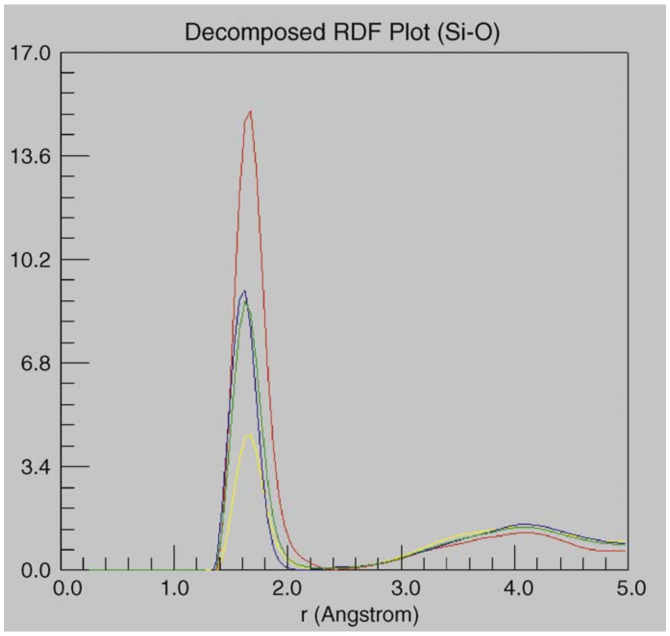

Fig. 3. RDF single plot: Decomposition of Si–O RDF according to the types of oxygen. The blue, red and yellow curves are for non-bridging, bridging and hydrous oxygen, respectively. The total RDF is shown by the green curve.

longer range than bonding does. Unlike coordination, bonding is defined between only those atomic pairs, which are chemically bonded and the distance should be always the minimum after the first peak. For instance, in hydrous silicate melt, chemical bonds exist between Si and O, Mg and O, and O and H atoms.

For a crystal, the bulk nearest neighbor coordination numbers are well defined and their values for a given atomic species pair are usually the same irrespective of the locations of the atoms. However, coordination is not same everywhere in a defective crystal or at surface and interfaces. The surface coordination number is always less than the bulk coordination number and is also dependent on which Miller index the surfaces use; for example, in a bcc crystal, the bulk coordination number is 8 whereas the 100 surface coordination number is 4. Similarly, the coordination number near a vacancy site or grain boundary may be smaller than the bulk value. Coordination is much more diverse in liquids and glasses; it is a function of both space and time. For instance, Si–O coordination numbers of all the silicon atoms in a silicate liquid are not necessarily the same. Since all atoms in the liquid are constantly moving, the coordination number of a silicon atom does not remain constant with time. It represents an instantaneous value, which may vary from one snapshot to another. In this sense, it is generally preferable to calculate a mean value by using $g_{\alpha\beta}$ (Eq. (5)) which itself is obtained by averaging over all atoms of two species under consideration and over a finite simulation period

In a multi-component system containing s species, one can have s^2 coordination types—multivariate information represented by an asymmetric square matrix of order s:

$$\begin{vmatrix} \mathrm{ce}_{12} & \mathrm{ce}_{12} & .. & \mathrm{ce}_{1s} \\ \mathrm{ce}_{21} & \mathrm{ce}_{22} & .. & \mathrm{ce}_{2s} \\ : & : & : & : \\ \mathrm{ce}_{s1} & \mathrm{ce}_{s2} & .. & \mathrm{ce}_{ss} \end{vmatrix} \tag{6}$$

Here, each term $\mathrm{ce}_{\alpha\beta}$ represents the coordination environment of species α with respect to species β in terms of a single number ($C_{\alpha\beta}$) in the average sense. The diagonal terms represent like-atom coordination whereas the off-diagonal terms represent unlike-atom coordination. For example, with $s = 4$ for hydrous magnesium silicate liquid, there are 16 different partial environments. Both the RDF and mean coordination have limitations as being isotropic so it is important to supplement interpretation of these functions with other structural information by exploring individual snapshots. One way of doing this is to decompose each coordination environment ($\mathrm{ce}_{\alpha\beta}$) into a variety of coordination species, which depend on space (i.e., vary from atom to atom) and time (i.e., vary from snapshot to snapshot).

3.2.1. Partial coordination environment

The coordination environment of an individual atom in the system at a given time instant represents the distribution of other particles around it. In particular, we are interested to know in the immediate neighborhood of each atom i of type α how many other atoms (labelled as j) of type β can be found and how they are arranged. The neighborhood chosen for coordination is simply a spherical region of radius $r_C = r_{\min}^{\alpha\beta}$ and all particles of type β falling in this neighborhood are taken into account. The partial coordination environment of an atom (labelled as i) at time t is thus defined by

$$\mathrm{nn}_i^{\alpha\beta}(t) = \{1 \le j \le N : d(i,j) \le r_{\min}^{\alpha\beta} \wedge \mathrm{type}(j) = \beta\} \tag{7}$$

where N represents the total number of atoms in the system. Thus in a multi-component system, each term in the matrix representation of an instantaneous coordination environment becomes

$$\mathrm{ce}_{\alpha\beta}(t) = \{\mathrm{nn}_i^{\alpha\beta}(t) | \forall\, i \in N_\alpha\} \tag{8}$$

For each pair of species, a unique coordination environment exists. The corresponding snapshot contains coordination information of all atoms of species α with respect to the atoms of species β at time t (Fig. 4). In the ball-and-stick representation, each coordination snapshot is visualized by displaying atoms of both species under consideration as spheres and by connecting central atoms (i's) with all of their coordinated atoms (j's) by lines. The numbers of lines emanating from the central atoms represent the corresponding coordination numbers $|\mathrm{nn}_i^{\alpha\beta}(t)|$'s. The central atoms are rendered with colors selected from a color map in which the color represents the coordination number (Fig. 5, left).

In some cases, the local coordination environment can be better expressed as polyhedral units. For instance, four-fold coordination means a tetrahedron with the type α atom being at the centre and surrounding type β atoms at the vertices of the tetrahedron. The coordination polyhedra are computed using Qhull algorithm [20]. The number of vertices in the polyhedron is equal to the coordination number of the atom, which is assumed to be at the centre of polyhedron. The color of the polyhedron encodes the coordination number (Fig. 5, right). The links between the central atom and the vertex atoms can be also drawn with an option of the length information encoded. An advantage of the polyhedral representation is that we can study other properties of this structural unit. Polyhedra are rarely perfect (regular). The degree of polyhedral distortion can be characterized in terms of quadratic elongation and bond-angle variance [21,22], which are defined, respectively by

$$\lambda_i^P = \sum_{k=1}^{\mathrm{nn}_i} \left(\frac{(l_k/l_0)^2}{\mathrm{nn}_i} \right) \quad \text{and} \quad \sigma_i = \sum_{k=1}^{\mathrm{nn}_i} \frac{(\theta_k - \theta_0)^2}{(\mathrm{nn}_i - 1)} \tag{9}$$

Here l_0 and θ_0 are bond lengths and angles in regular polyhedra, respectively. l_0 is computed as the average of all lengths forming a polyhedron. There are fixed angles only for a few regular polyhedra; for instance, $\theta_0 = 109.47^\circ$ for $\mathrm{nn}_i = 4$ (tetrahedron) and $\theta_0 = 90^\circ$ for $\mathrm{nn}_i = 6$ (octahedron) so the bond-angle variance can be calculated only for some cases. Fig. 6 shows that Mg–O

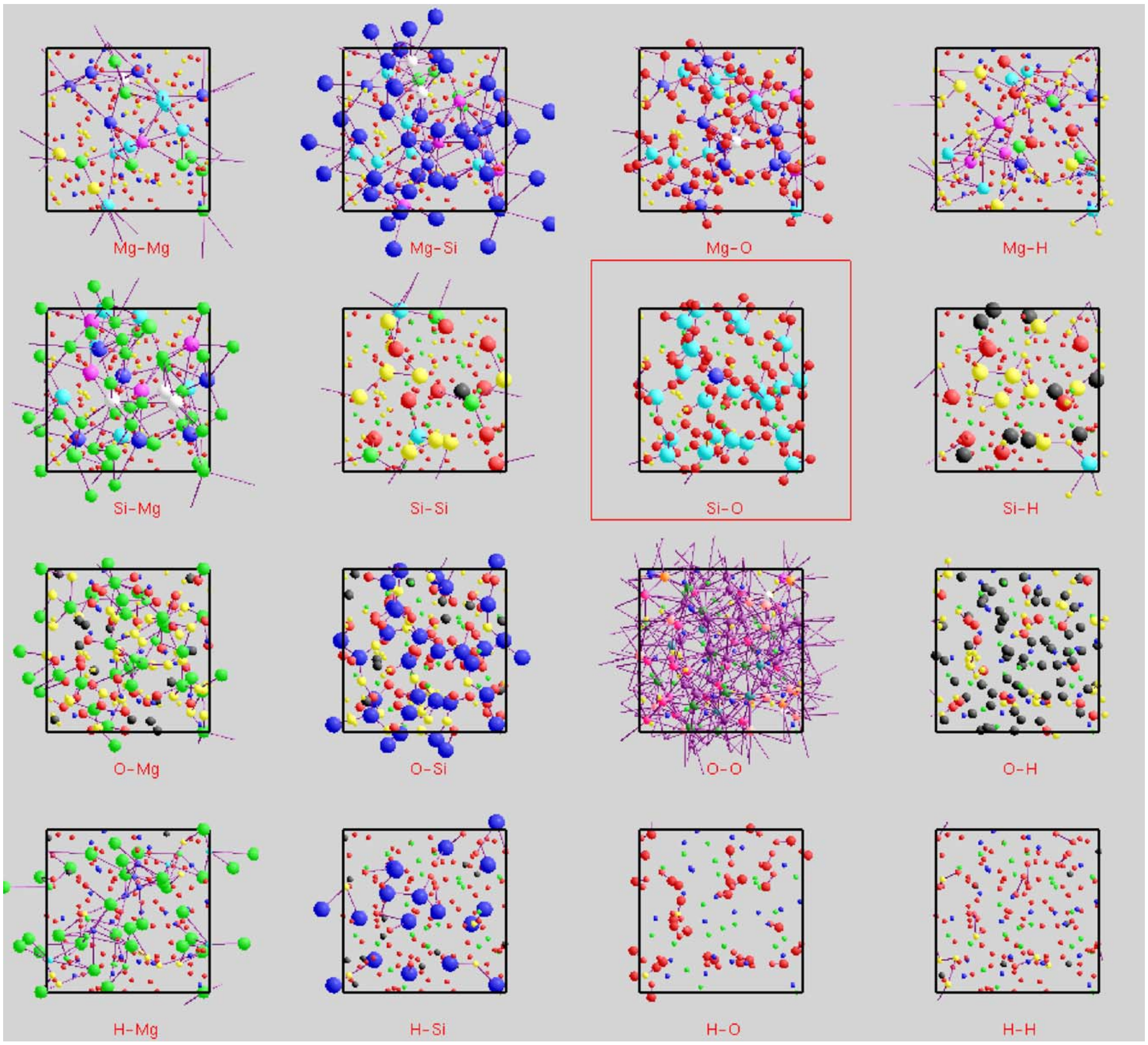

Fig. 4. Coordination matrix plot rendering sixteen different coordination environments in the hydrous silicate liquid. In each entry, atomic species pairs involved in coordination are drawn as spheres (connected by lines) and the color (of center spheres) encodes coordination number ($|\mathrm{nn}_i^{\alpha\beta}(t)|$). The coordination numbers of 0, 1, 2, 3, 4, 5, 6 and 7 are, respectively, represented by black, red, yellow, green, cyan, blue, magenta and white. The cutoff distances are taken from the RDF matrix plot. The atomic species not contributing to coordination are shown by tiny spheres with their respective colors (Mg: green, Si: blue, O: red and H: yellow).

polyhedra are more distorted than Si–O polyhedra in the silicate liquid. Another relevant quantity is the polyhederal volume, which varies between polyhedra of the same or different types. It is important to note that coordination can be also represented using other types of polyhedra obtained by using the Voronoi construction method [10]. Such polyhedra are computed by finding the planes, which enclose the set of points that are closer to the central atom than to any other atom. Unlike the coordination polyhedra studied in this study, the Voronoi construction may include the contributions from the second coordination shell and does not directly represent the coordination number. For example, a six-fold Si–O coordination state maps to a cubic Voronoi polyhedron rather than to an octahedron (six O atoms at the vertices and Si atom at the center). A detailed analysis of Voronoi polyhedra was previously carried out for amorphous silica [10].

3.2.2. Mixed coordination environment

A coordination matrix (or row or column) plot renders simultaneously more than one partial coordination environment using separate viewports (Fig. 4). While it allows us to compare different environments with each other, it is also desirable to render the coordination environments among multiple pairs of species in the same viewport. Such a mixed plot is expected to be useful in exploring how different coordination environments complement with each other to define the overall structure of the system in question. For instance, visualization snapshot consisting of color-coded Si–O coordination polyhedra, and O–H and H–O coordination spheres can assist in the identification of different forms of water speciation (Fig. 7). However, using a single viewport to simultaneously render multiple coordination environments has a limitation. An element in the coordination matrix specifies coordination environment of the species defined by the row with respect to the species defined by the column. When multiple environments are visualized together in the same viewport, only one coordination environment from a row can be rendered because one row corresponds to one species, and spheres representing the atoms of this species can be color-coded in only one way to convey the coordination information. Conversely, multiple coordination

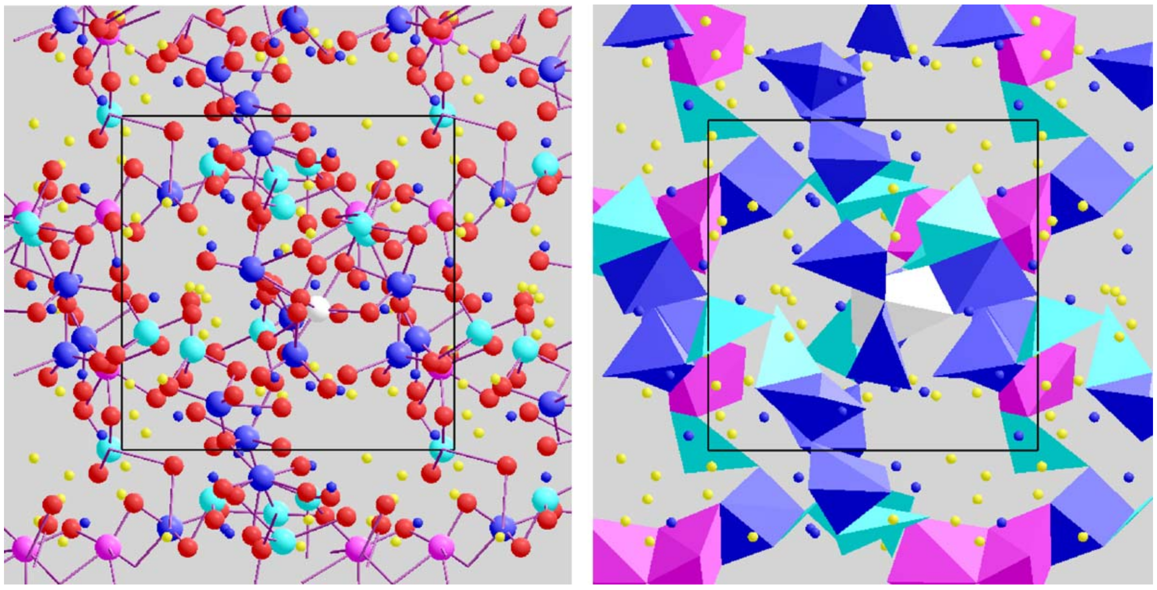

Fig. 5. Ball-and-stick (*left*) and polyhedral (*right*) representation. Mg–O coordination information is encoded by the colors of spheres and polyhedra. The coordination numbers of 0, 1, 2, 3, 4, 5, 6 and 7 are, respectively, represented by black, red, yellow, green, cyan, blue, magenta and white. The noncontributing atomic species are silicon (blue tiny spheres) and hydrogen (yellow tiny spheres).

environments from one entire column can be selected for a mixed coordination snapshot. The limitation can be modelled using a directed graph, *D* in which vertices are the atomic species and the edges are the coordination relationships between the corresponding pairs of species (Fig. 8). The graph can also contain a loop in it when coordination of a species with respect to the same species is selected. For the graph to be practically useful, each vertex must have only one outgoing edge although it can have many incoming edges. In Fig. 8, each vertex has only one outgoing edge so this is a valid graph for mixed coordination representation.

3.2.3. Coordination stability

Coordination varies from one snapshot to another. For a given snapshot, the atomic configuration is composed of various coordination species since coordination varies from one atom to another of the same species. It is important to explore the time dependence of these coordination states. We define the stability of a coordination environment for a particle *i* as the fraction of time the environment exists in the system. The stability consists of two components: the stability of the coordination number and the stability of the coordinated atoms. An atom can have the same coordination number even when it gets coordinated with different set of neighbors at different instants. Let $c_i = \left|\mathrm{nn}_i^{\alpha\beta}(t)\right|$ be an instantaneous coordination number for atom *i* at time *t*. This number is an integer for individual atoms because at any instant, either one atom is coordinated with another atom or it is not coordinated. Two atoms cannot be partially coordinated. So, over *N* snapshots, we track atom *i* to find the fraction of the time it is coordinated with $c_i(t)$ atoms. Let this fraction be $f[c_i]$. Then, c_i and $f[c_i]$ are visually represented, respectively, by the color and size of the sphere representing the central atom (Fig. 9). For an atom *i* of species α, the nearest neighbors of species β at time *t* are given by

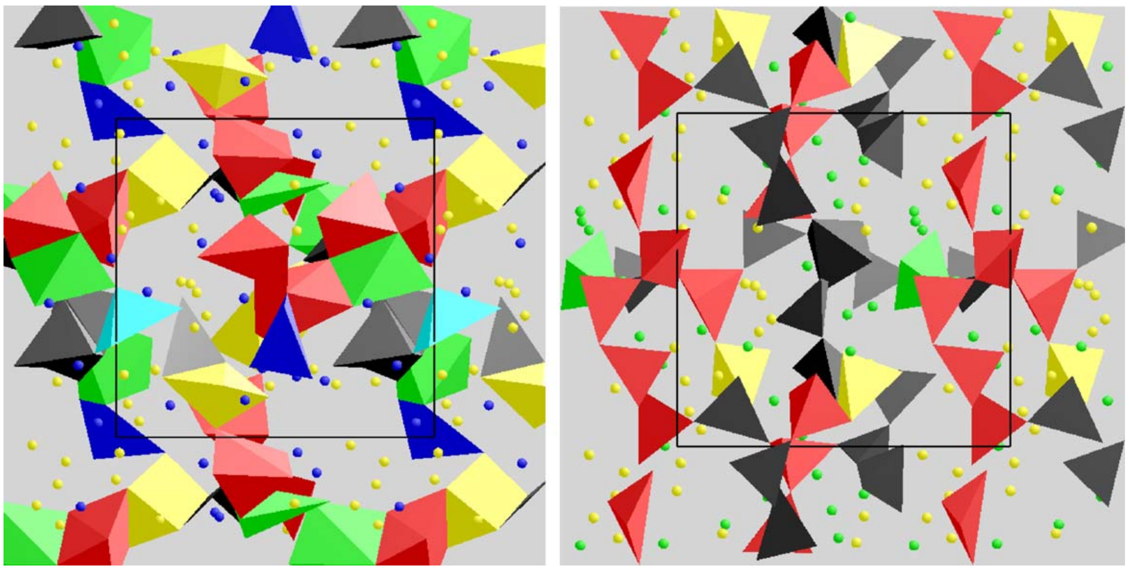

Fig. 6. Quadratic elongation information of Mg–O (*left*) and Si–O (*right*) coordination polyhedra. The polyhedra in *left* are relatively more distorted than those in *right*. The value increases in the order of black, red, yellow, green, cyan, blue, magenta and white.

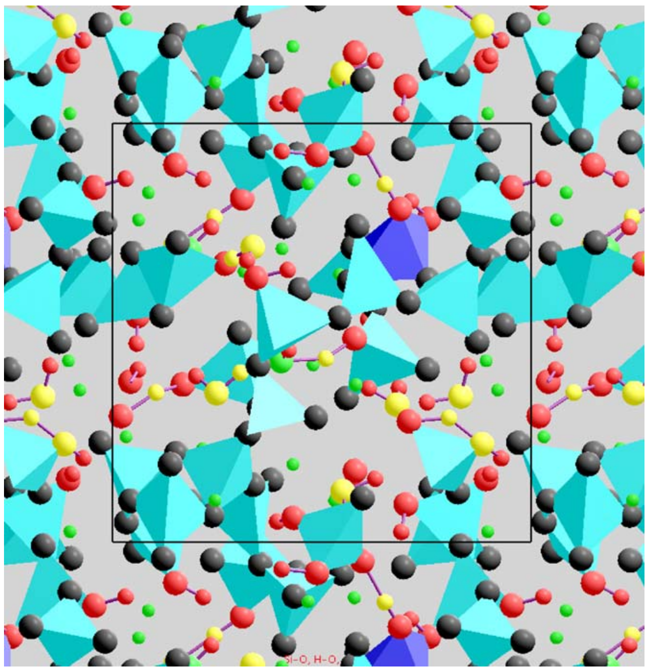

Fig. 7. Mixed coordination plot displaying the Si–O, O–H and H–O coordination environments together. Hydroxyls, water molecules, polyhedral bridging, edge decoration, and four-atom sequences are present. The coordination numbers of 0, 1, 2, 3, 4, 5, 6 and 7 are, respectively, represented by black, red, yellow, green, cyan, blue, magenta and white colors.

$\mathrm{nn}_i^{\alpha\beta}(t)$. Then, the set of all the atoms of species β that get coordinated to the atom i during an extended period of N steps is thus:

$$\mathrm{NN}_i^{\alpha\beta} = \bigcup_{j=0}^{N} \mathrm{nn}_i^{\alpha\beta}(j\Delta t) \tag{10}$$

Let $f_i(k)$, where $k \in NN_i^{\alpha\beta}$, is the fraction of time the atom k is coordinated with atom i. Then, when the atom k gets coordinated with atom i, $f_i(k)$ is used to represent the stability of this coordination relationship, which is encoded by the width of the bonds (Fig. 9).

$$\begin{tikzcd}
 & s_2 \arrow[d, bend right, dotted] & \\
s_1 \arrow[ur, bend left, dotted] & & s_4 \arrow[dl, bend left, dotted] \\
 & s_3 \arrow[u, bend right, dotted] &
\end{tikzcd}$$

Fig. 8. Graph model of mixed coordination environment.

The set of atoms, which are coordinated with the central atom under consideration during a selected temporal interval are referred to as a coordination cluster (Fig. 10). In any snapshot, this cluster comprises of those atoms that are currently coordinated to the central atom and those atoms that have contributed to the coordination at some other time (before or after the current instant). Visualization differentiates the two types of contributions by using different color or thickness for the connecting lines between the central atom and contributing atoms. Each atom of species α forms its own coordination cluster, which can be rendered separately or together with all other such clusters.

The stability of a polyhedral surface is harder to visualize than the stability of individual bonds. This is because we are actually trying to visualize the effect of more than one bond and somehow represent the cumulative effect of all those bonds in one object at the same time. For this purpose, we first define the stability of the surface as $s_\mathrm{p} = \prod s_\mathrm{bond}$, where s_bond is the stability of individual bonds defined as the fraction of the time it exists in the dataset. As each of the bonds has to exist simultaneously to form the polyhedral structure, we multiply the stabilities of individual bonds to compute the stability of the polyhedron as a whole. One way to represent the polyhedral stability is to modulate the polyhedral surface itself using s_p as the modulating quantity and the other way is to vary the color intensity accordingly (Fig. 11). Such modulation of shape or intensity variation tells us about the

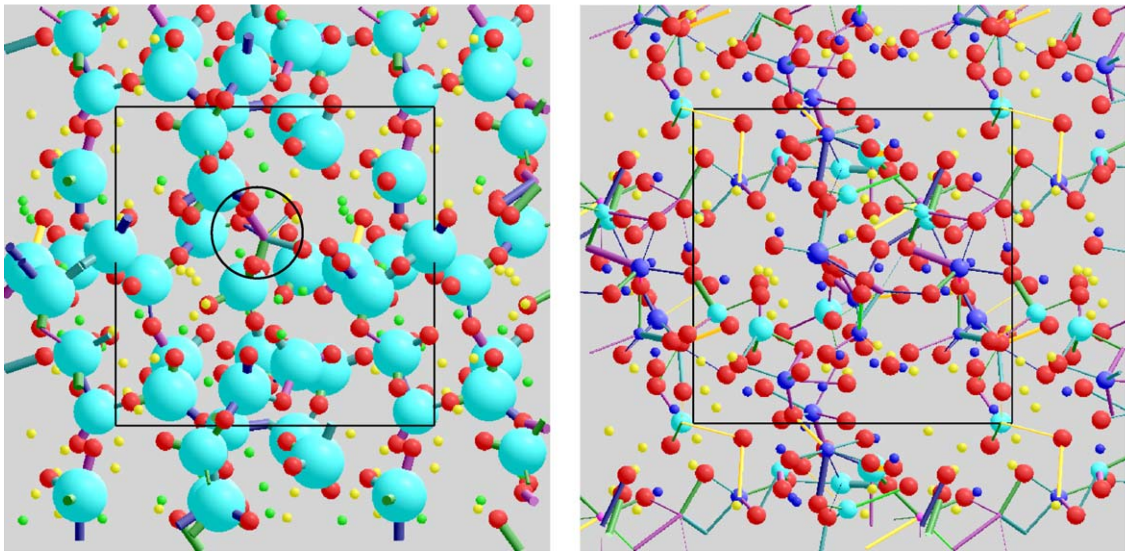

Fig. 9. Stability of Si–O (*left*) and Mg–O (*right*) coordination. Large spheres and thick bonds in *left* suggest that the four-fold state (cyan) for Si–O coordination is highly stable and dominates the coordination environment. A five-fold coordination state (blue) hardly exists (marked). The color and size of bonds encode the length and stability of the bond, respectively. On the other hand, the Mg–O coordination (*right*) consists of various states with a wide range of stabilities.

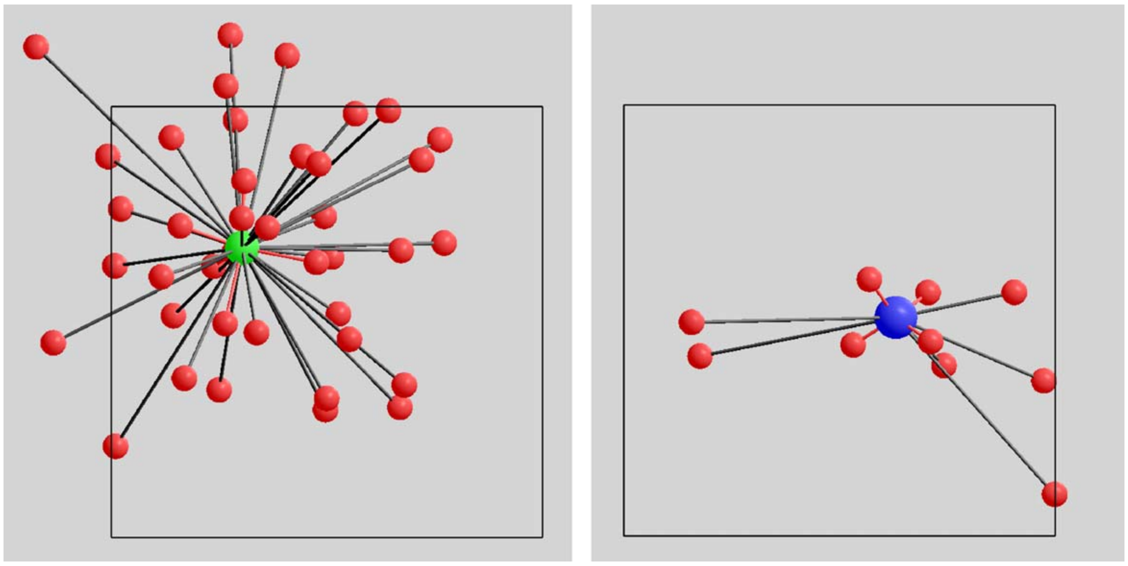
Fig. 10. Coordination cluster of one Mg (*left*) and one Si (*right*) atom. The coordination is with respect to O atoms (red spheres). The red lines indicate the oxygen atoms coordinated with the central atom at the current snapshot so the number of red lines gives the current coordination state of the atom.

overall stability of the polyhedral object as a whole but it does not tell us why the object is stable or unstable. Also, as only size variation is quantitative, change in shape will not be able to convey the quantitative information that we want to convey. It also does not tell us anything about which atom(s) is (are) more likely to detach from the surface than the others or which atoms are likely to be bound with the surface more strongly than the others. Instead of modulating the shape, we modulate the size of the coordinated atom to visualize the probability of their coordination [13]. Probability of coordination of atom k with another atom i is given by $f_i(k)$.

3.3. Cluster structures

3.3.1. Nearest neighbor cluster

An atom i is said to be a nearest neighbor of another atom j, if $d(i,j) < r_C$, where r_C is the cutoff distance. If we can traverse through a group of atoms following a path from one atom to another atom such that the distance between any two consecutive atoms on the path is within the cutoff, we obtain a cluster which connects successive nearest neighbor atoms. This is referred to as a nearest neigbor (NN) cluster. Let $\text{nn}_i = \{1 \leq j \leq N_\alpha : d(i,j) \leq r_c\}$ be the set of the nearest neighbors of the atom i. The NN cluster structure formed by the atom i can be defined as $i \cup K$, where K is recursively defined as $\{i\} \cup \{\text{nn}_j \ \forall \ j \in K\}$. The breadth-first or depth-first traversal of a graph data structure $G(V,E)$ in which each atom is represented as a vertex and the atomic pair which are within the cutoff distance is represented as an edge yields the desired cluster. The cluster contains all the atoms that are reachable from any atom in it. The NN cluster is rendered as the new atoms are found instead of first saving the cluster separately.

3.3.2. Common neighbor cluster

A common neighbor cluster for a given pair of atoms is the set of all the atoms that are the nearest neighbors of both the atoms in the pair. This method represents a way of decomposing the first and second peaks of RDF according to the local environment of each atomic pair that contributes to the peak structures [23,24]. An

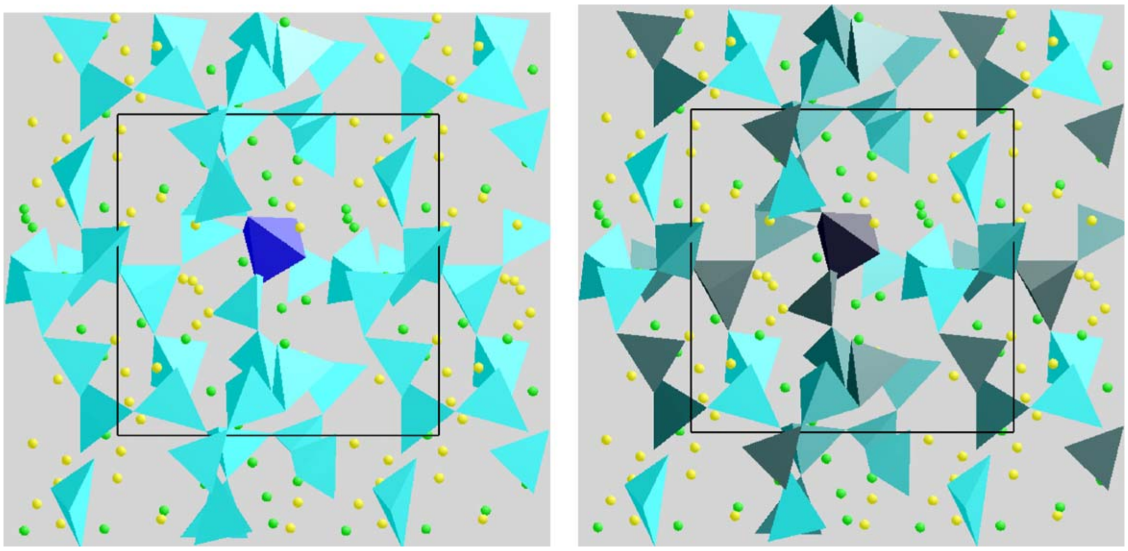
Fig. 11. Si–O coordination polyhedra (*left*) and their stabilities coded by intensity (*right*). The blue polyhedron (i.e., a five-fold coordination species) in *left* becomes the least stable (the darkest in the *right*).

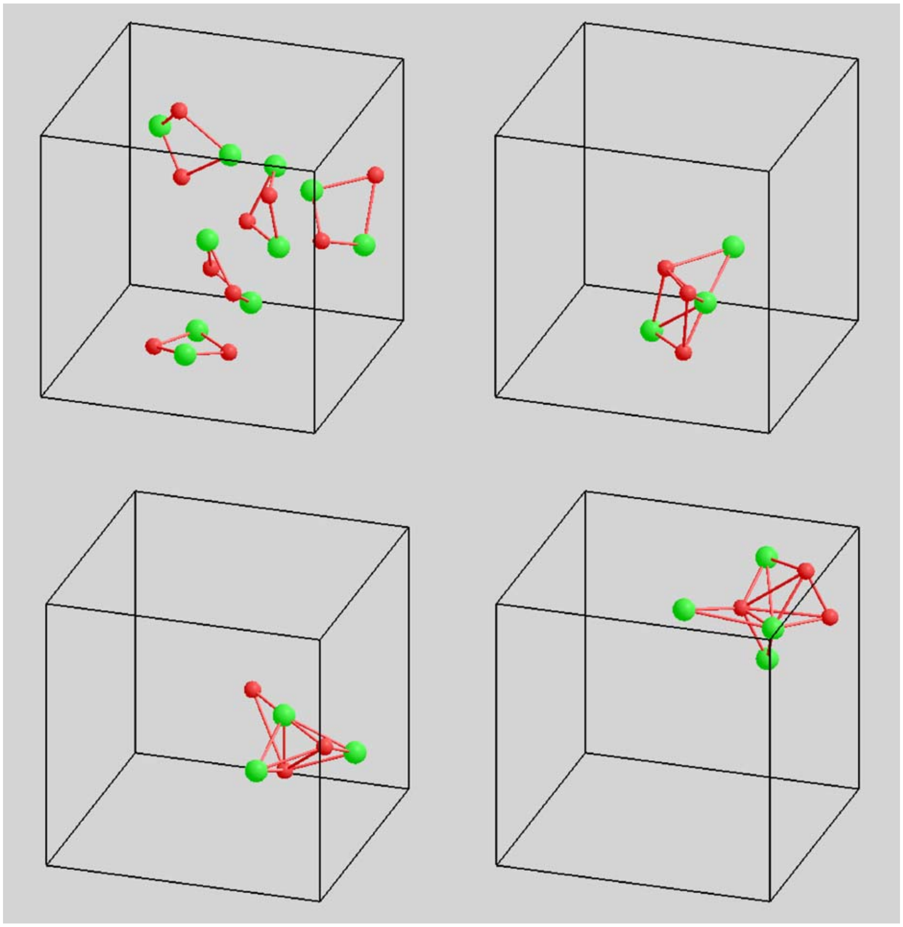

Fig. 12. Common neighbor clusters containing two, three (mixed), four and five common neighbors for cutoff distances of 2.5, 2.7, 2.9 and 3.1 Å in MgO liquid.

atom k is said to be a common neighbor to i and j, if $d(i,k) \leq r_c$ and $d(j,k) \leq r_c$, where r_c is the cutoff distance. For a pair of atoms i and j, let $cn = \{k \mid d(i,k) \leq r_c \wedge d(j,k) \leq r_c\}$ be the set of common neighbors. Then, $cn \cup \{i,j\}$with all the coordination relationship among these atoms within the critical distance r_c is called the common neighbor cluster for atoms i and j. In particular, we are interested to calculate the number and properties of common nearest neighbors of the pair under consideration. These information helps us to identify atoms in particular environment such as face-centered cubic, hexagonal close-packed, body-centered cubic or icosahedron. Different types of pairs are associated with different types of local order. There exist other methods (not considered here) for characterizing the state of a local crystal structure in a material system such as one based on computation of common atomic neighborhood parameter [25].

We find the common neighbor clusters using a graph data structure $G(V, E)$ in which each atom is represented as a vertex and the atomic pair which are within the cutoff distance is represented as an edge. Note that if two vertices are separated by more than two edges, then they cannot share the same neighbors. Cluster computation involves two steps. In the first step, the graph is traversed to find all the pairs of vertices, which are not farther than two edges. This also finds those pairs that have at least one neighbor common to each other. For all vertices, i, in the adjacency list of every vertex v, it checks whether we already know some of its other nearest neighbors. If we do, then we have found a common neighbor to some pairs of vertices and this vertex is added to the common neighbor of each of those pairs. The vertex, v, is also added to the nearest neighbor list of vertex, i. At the end we have common neighbor lists for all pairs that have at least one neighbor common between them. The second step then finds the subgraph spanned by the set of common neighbors. The subgraph and the corresponding vertex-pair together constitute the common neighbor cluster. So the common neighbor cluster is the intersection of the coordination environments of the two vertices. Fig. 12 shows the computed clusters of different sizes for MgO liquid.

3.4. Ring structures

Ring structures are used to understand the medium range order. The ring statistics are widely used to analyze the structural properties of amorphous solids, liquids and nanomaterials [9,16,26,27]. The arrangements of the rings formed by the atoms can describe the topology of these systems. There are different definitions of rings available in the literatures and the ring statistics differ according to the definitions [9,28–31]. Software systems are also available for offline ring analysis [32]. Finding all rings in a system is computationally intensive because the ring computation contains Hamiltonian cycle problem as a special case and there are possibly an exponential number of rings in the system. Considering all rings in the system is not practical for relatively large systems. The maximum ring size can be restricted to a physically relevant size instead of trying to compute all the possible rings. A finite-size supercell used in the simulation is first replicated to find the largest possible ring. This process makes multiple copies of an atom and assigns each of them a unique *id*. Thus, rings are kept as lists of atoms arranged in parent-child relationship where each atom is accompanied by its position in the replicated system and its original atomic *id*. The atomic *id*'s in the original system have to be mapped from the replicated *id*'s. Let r_i be a new index for an atom i in the replicated system and *rf* is the replication factor. Function to convert the original index to a set of replicated indices, R_i, is:

$$R_i = \{rf \times i + j | 0 \leq j < rf\};\ \ r_i \in R_i \qquad (11)$$

So, one index is replicated to *rf* unique indices and the atomic *id* (i) in the original atomic system is computed from r_i as: $i = r_i/r_f$.

Suppose $G = \{V,E\}$ is the graph with vertex set V and edge set E. For any two vertices x and y in V, if there is a sequence of vertices, $p = v_1, v_2, \ldots, v_n$ such that $(v_i v_i + 1) \in E$ for all $1 \leq i \leq n{-}1$, $x = v_1$, and $y = v_n$, then p is a path between the vertices x and y. The length of the path is equal to the number of edges in the path. A path between two vertices x and y is a cycle if vertices x and y are the same. If every vertex in the cycle except one vertex appears exactly once and the one that appears more than once appears exactly twice, then the cycle is called a simple cycle. There are two distinct paths (of not necessarily equal lengths) between any two vertices in the cycle. The shortest path between two vertices can be defined with respect to the graph, G, or with respect to a cycle. If the shortest path between v_i and v_j with respect to the simple cycle is not greater than the shortest path between those two vertices with respect to the graph G, then the cycle c is a primitive ring. Thus, a ring is primitive if another shorter path between any two vertices in the ring other than the shortest path in the ring itself between those two vertices does not exist. Local ring structure for a vertex v_i is defined as a set of primitive rings of which v_j is also a part: $R(v_i) = \{c | v_i \in c\}$. This is the typical definition used to calculate ring statistics in a material system. Thus, only the primitive rings are of interest and large rings are less likely to be primitive as they usually have shortcuts.

We first give a brute force approach [9] for the ring computation. A logical cluster data structure for each atom in the system is constructed from the graph of the complete system (Fig. 13). It stores the information about all the atoms reachable at different levels from the atom. The main idea behind the brute force approach is that whenever there is one vertex at the same level in two different places in the cluster structure, and if this is the case, then there must be two unique paths to that vertex starting from the root. A ring can be formed joining the two paths. For large rings, there are many different paths between the vertex and the root, and the number of possible paths in a graph increases exponentially with the ring size. When there are n different paths, then any pair of paths can make a ring so there are $n(n-1)/2$ different possible rings. However, all the rings may not satisfy the primitiveness criterion. A large number of rings have to be checked for their primitiveness when the ring size is large.

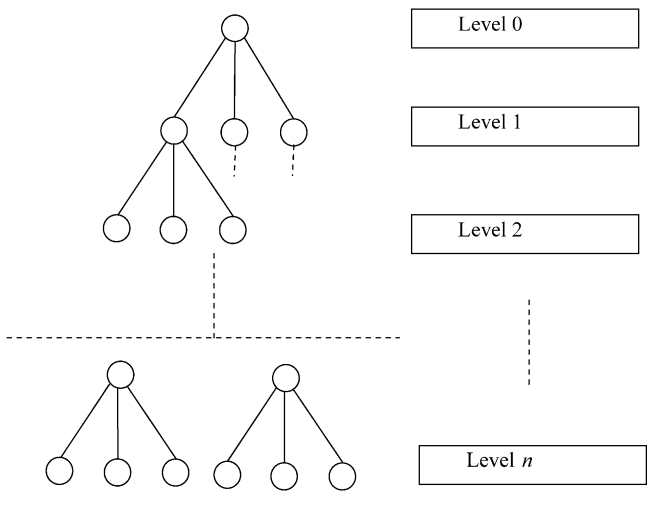

Fig. 13. Cluster data structure for vertex i.

Due to an exponential increase in the number of possible paths and also the size of the cluster structure itself, the brute force algorithm becomes computationally intensive for large systems. At each level, there will be an exponential number of atoms and information that needs to be stored also becomes exponential for large rings. However, all the data need not be stored for efficient computation of the primitive rings set. To reduce the redundant information, the cluster data structure is explicitly split into two separate data structures: a graph and a shortest distance map. Such restructuring of the data structure results in a better algorithm [30]. The improved algorithm first computes shortest distance maps, S_{map}, for all the vertices in the graph. Then all the vertices (m_i) at a distance $r_{\text{size}}/2$ from vertex i are computed. If any of the vertices in m_i has more than one distinct path to the vertex i, then there is possibly a primitive ring. So, all the paths from each middle vertex to the vertex i are found. For each pair of paths, a possible ring is formed and checked for its primitiveness. The computational cost of checking whether a ring is primitive is reduced by limiting the number of pair of vertices checked. We use the mid-node theorem [33] that states, "For any primitive even 2n-ring, between any check-node and its mid-node, the two equal paths with n links along the ring must be the shortest." If the ring is primitive, then it is added into the set of primitive rings. The algorithm described is valid for finding even-sized rings.

The rings are stored as lists of atom indices and positions. They are visualized using the standard ball-and-stick representation (Fig. 14, left). Superimposed on this is rendered a surface generated by a set of triangles for each ring (Fig. 14, right). Consider a ring, $R = \{r_j | 1 \leq j \leq |R|\}$, for vertex i, such that r_k is the parent of r_{k+1} for $k \geq |1$ and $r_{|R|}$ is the parent of r_1. The triangle is calculated by taking a set of three vertices, where one vertex is r_1 and remaining two vertices are r_k and r_{k+1} where $2 \leq k \leq |R|{-}1$. The normal for each triangle is calculated separately. The triangulation algorithm treats individual rings independently. Being computationally intensive, the ring algorithm is implemented to run in separate thread from the main application thread. To achieve interactive visualization of ring structures, the rings are computed for the selected atom for the current time step only. However, finding the ring statistics involves computation of rings for all the atoms averaging over multiple steps. Fig. 15 shows the Si–Si ring structure of silica liquid as the maximum ring size used in the computation is varied from 2 to 12. The ring structure for the cutoff size of 12 consists of eight rings, which include those found for the smaller cutoff sizes.

4. Visualizing dynamical properties

The information on atomic configuration from a MD simulation is time ordered and is commonly visualized using the methods like animation and pathlines. The animation method renders atomic configuration at each time step at a time whereas the pathlines method displays the complete trajectories of all atoms by rendering the atomic positions at all successive time steps. While such representations do not discard any information, the animation presents an instantaneous picture whereas highly entangled trajectories are difficult to interpret. There are other ways of understanding the dynamics as presented here. Various kinds of displacement data are extracted to understand the extent and nature of the movement of the atoms.

4.1. Diffusion coefficients

Assuming that the simulation dataset in question consists of only atomic positions, we can use the Einstein relation to compute

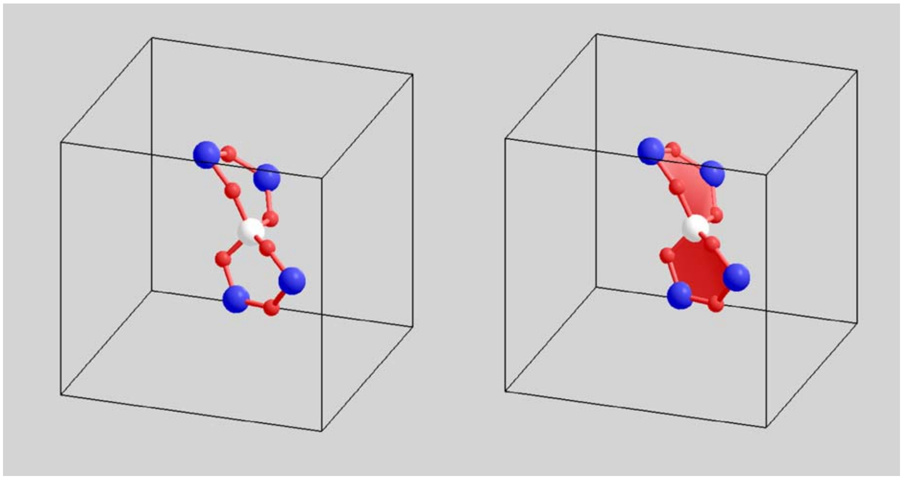

Fig. 14. Si–Si ring structure for a silicon atom (large white sphere) in silica liquid. It contains 2 three-membered rings; each ring consisting of three silicon atoms (one large white sphere and two large blue spheres). The oxygen atoms (small red spheres) bonded to silicon simply form link between two successive silicon atoms and are not counted in determining the ring size. On the *right*, a surface is added. Three Si atoms and three O atoms lie on different planes.

self-diffusion coefficient for each atomic species [8] as follows:

$$D_\alpha = \lim_{t\to\infty}\frac{\left\langle [r(t)]^2\right\rangle}{6t}, \quad \text{where } \left\langle [r(t)]^2\right\rangle = \frac{1}{N_\alpha}\sum_{i=1}^{N_\alpha}|r_i(t+t_0)-r_i(t_0)|^2 \qquad (12)$$

is the mean square displacement (MSD). The positions of the *i*th atom at time origin t_0 and then after time t are $r_i(t_0)$ and $r_i(t+t_0)$, respectively. Translational symmetry of the system is accounted for so that the MSD value is not restricted by the size of the supercell. The partial MSD was calculated by averaging over atoms of a given species. To get a better statistics, MSD is averaged over different time origins, t_0's. MSD curves are extracted and rendered. One could plot these curves for individual atoms separately or the total MSD for different time origins. Alternatively, the integrals of the time-correlation functions for velocities can be used to compute diffusion coefficients. Similarly, other types of the time-correlation functions can be computed depending on the simulation outputs.

4.2. Pathlines

A pathline or trajectory represents the actual movement of atoms in space during a finite time of simulation. In a solid system,

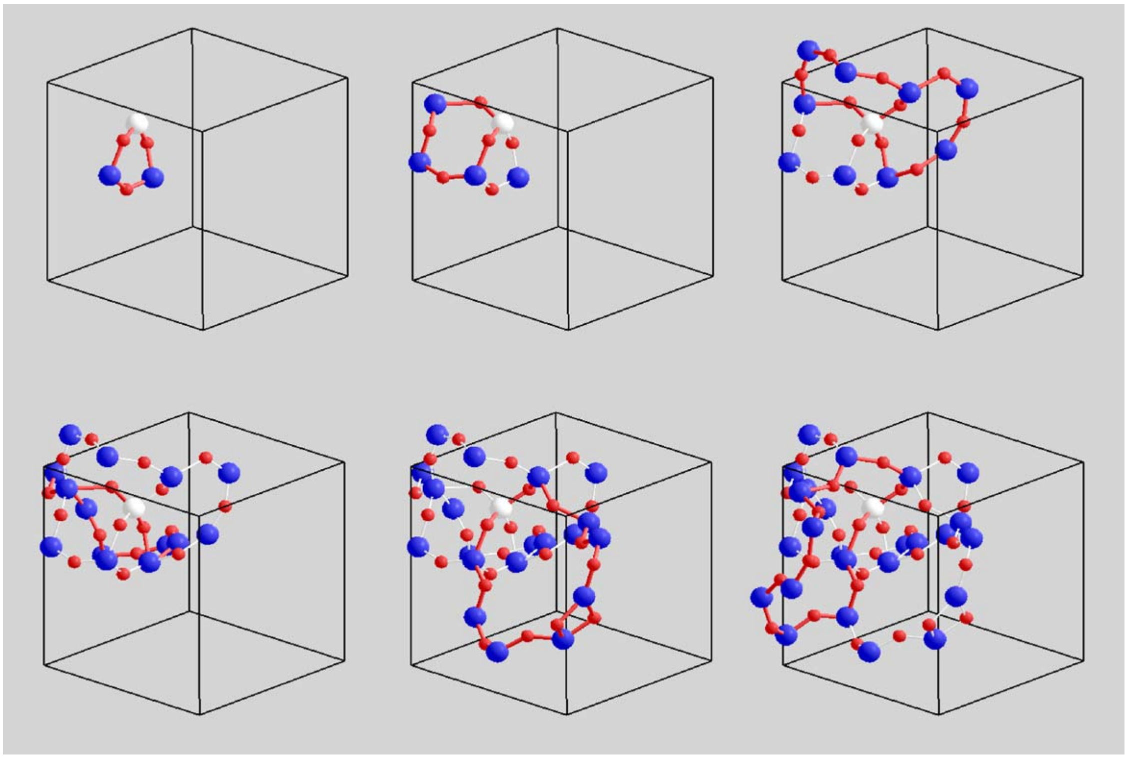

Fig. 15. Different sizes of Si–Si rings bonded via oxygen atoms (red spheres) in silica liquid. The 3-, 4- and 5-membered rings (the upper row), and 8, 9- and 10-membered rings (the bottom row) are highlighted with thick red bonds.

each atom remains confined within a small region around its equilibrium position and the trajectories of different atoms do not overlap. In a dynamical system on the other hand, atoms move a lot resulting in dispersed and overlapping trajectories. As an atom moves within the supercell satisfying the periodic boundary conditions, it can be traced using a color-coded line. The pixel color at a given position is varied according to the elapsed time or the distance travelled by the atom relative to some reference position. The pathlines are used to visualize the raw movement of individual atoms (Fig. 16) and those forming a well-defined structural unit such as a polyhedron and its stability [12].

4.3. Atomic displacements

Various sets of displacement data are generated to characterize the extent and pattern of the atomic movement during simulation. In general, displacements are defined as $\Delta r_i = r_i^t - r_i^{t_0}$, for i = 1, 2, . . ., N. Here, r_i^t and $r_i^{t_0}$ are the positions of ith atom in a given (at a particular time) and reference configuration, respectively. The data may represent differences of a given atomic configuration (r_i^t) from the initial (r_i^0) or previous ($r_i^{t-\Delta t}$) or next ($r_i^{t+\Delta t}$) configuration. The reference configuration can be the crystalline configuration (r_i^{crys}) as well. The other relevant differences are those involving the mean positions $c_i = \frac{1}{n_{\text{steps}}}\sum_{j=1}^{n_{\text{steps}}} p_i^j$ taken over the whole simulation period, where n_{steps} is the number of simulation steps, p_i^j is position of ith atom at jth simulation step. All these data represent discrete vector data, which are rendered using spheres and lines (Fig. 17). The magnitude of the vector is represented by the size of the sphere placed at each atomic site (p_i) in 3D space: $r_i^s = f|\Delta r_i| + a$, where f is the scaling factor and a is the minimum radius given to each sphere. The direction is represented by a line segment with an arrow pointing away from the surface of the sphere:

$$\text{line}\left(|\Delta r_i|\, p_i, |\Delta r_i|\, p_i + l\frac{\Delta r_i}{|\Delta r_i|}\right) \tag{13}$$

where Δr_i is the orientation vector, p_i is the center of the sphere, and l is the length of the line. In the case, where we are interested at the farthest positions the atoms reach during the whole simulation period from the mean positions, the centroid spheres are drawn at c_i's with the radii defined by $r_i = \max_{j=1:n_{\text{steps}}}\{d(c_i, p_i^j)\}$.

4.4. Principal component analysis

The atoms do not move equally in each direction. Principal component analysis (PCA) [34] is used to analyze the overall extent and anisotropy of each atom movement. PCA usually assumes that data points are independent of each other. In strict sense, this is not the case for the position-time series as they remain highly correlated for long durations. By relaxing the requirement of probabilistic independence among the data points, PCA is expected to provide valuable information about the aggregate motion of individual atoms by reducing the dimensionality of a dataset that consists of a large number of interrelated variables. We define the covariance matrix for each atom, i, for a given dataset by

$$\Sigma_i = \begin{pmatrix} \sigma_i^{xx} & \sigma_i^{xy} & \sigma_i^{xz} \\ \sigma_i^{yx} & \sigma_i^{yy} & \sigma_i^{yz} \\ \sigma_i^{zx} & \sigma_i^{zy} & \sigma_i^{zz} \end{pmatrix} \tag{14}$$

The diagonal terms of the covariance matrix are the variances along three orthonormal axes (x-axis, y-axis and z-axis) and off-diagonal terms are the covariance between the two axes on the superscript. To compute the covariance matrix, the mean position

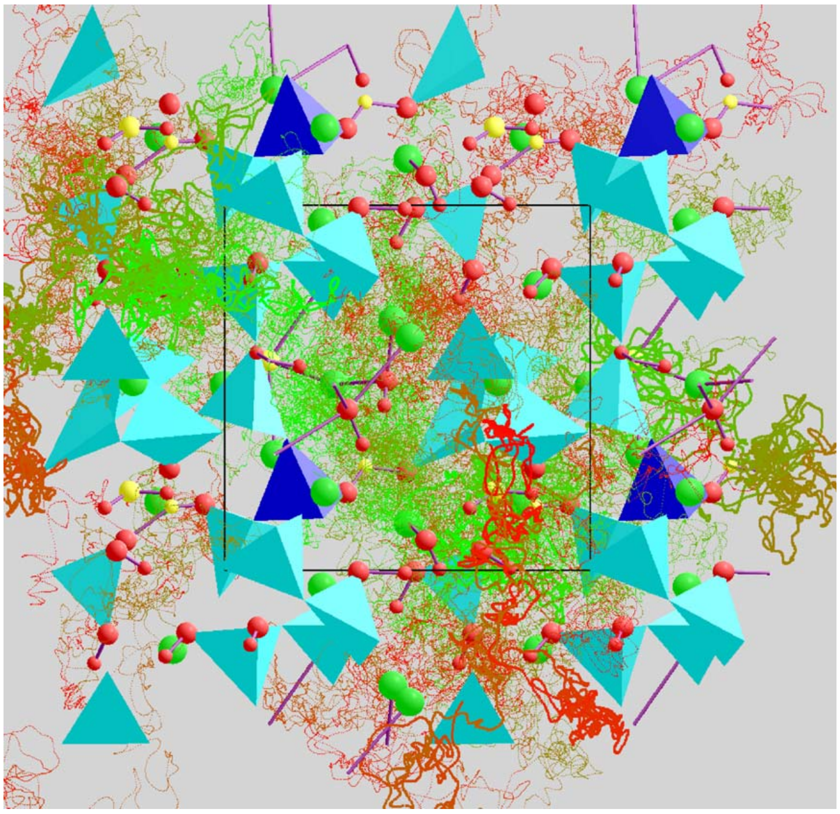
Fig. 16. Si–O coordination polyhedra (four-fold, cyan; five-fold, blue), hydroxyls (large red–small red pairs) and water molecules (small red–large yellow–small red triplets) with H atom pathlines (time-encoded over 10 ps, green to red) and Mg atoms (green spheres) in the background. Trajectories of two randomly selected H atoms are highlighted with bold pathlines.

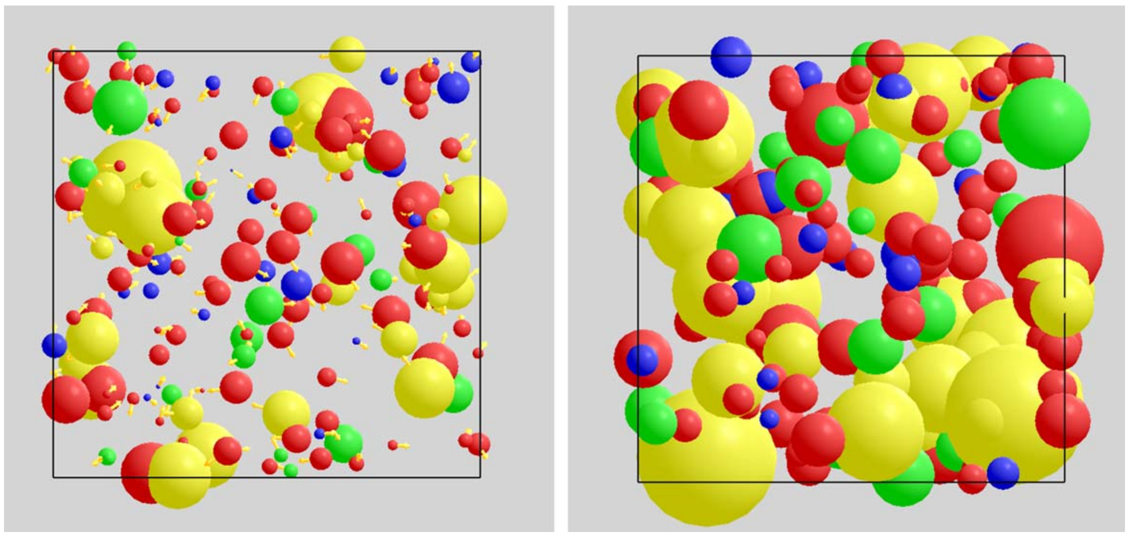

Fig. 17. Instantaneous (*left*) and averaged (*right*) atomic displacements in the hydrous silicate liquid. The instantaneous spheres are scaled up and the average spheres are scaled down from their actual sizes by a factor of 10.

of the particle is computed as,

$$\mu_i = \frac{\sum_{j=1}^{j=n_{\text{steps}}} p_i(j\Delta t)}{n_{\text{steps}}} \tag{15}$$

and the covariance and variances of the positional components are then computed as,

$$\sigma_i^{kl} = \frac{\sum_{j=1}^{j=n_{\text{steps}}} (p_i^k(j\Delta t) - \mu_i^k)(p_i^l(j\Delta t) - \mu_i^l)}{n_{\text{steps}}} \tag{16}$$

where k and l are two of the three positional components, x, y, and z. The covariance matrix is a symmetric matrix. Its eigenvalues and eigenvectors give the amount and direction, respectively, of the maximum variation in the data. For a positive semi-definite symmetric matrix, eigenvalues are real. Let the three eigenvalues and corresponding three eigenvectors be λ_1, λ_2, and λ_3, and υ_1, υ_2, and υ_3, respectively. Then we can define a principal component matrix, A, as:

$$A = \begin{pmatrix} \lambda_1\upsilon_1^1 & \lambda_1\upsilon_1^2 & \lambda_1\upsilon_1^3 \\ \lambda_2\upsilon_2^1 & \lambda_2\upsilon_2^2 & \lambda_2\upsilon_2^3 \\ \lambda_3\upsilon_3^1 & \lambda_3\upsilon_3^2 & \lambda_3\upsilon_3^3 \end{pmatrix} \tag{17}$$

Now, let's transform the position set, $p_i(t)$, by A as $p_i'(t) = A\,p_i(t)$. The transformed positions are defined with respect to the frame reference specified by the three orthogonal eigenvectors. These positions have the maximum variation along the υ_1 axis and successively decreasing variations along υ_2 and υ_3 axes. The ellipsoids are used to visualize the eigenvalues and eigenvectors of the covariance matrices (Fig. 18). We use λ_1, λ_2, and λ_3, as the major, medium and minor axes, respectively, of the ellipsoid and use eigenvectors, υ_1, υ_2, and υ_3, to construct a rotation matrix to orient the ellipsoid. The principal components are uncorrelated with each other so they form an orthogonal frame of reference. When the set of eigenvectors are not unit vectors, their values are normalized to provide an orthonormal frame of reference for the ellipsoids. The mean position of the set of positions is the center of each ellipsoid.

5. System design and implementation

A number of analysis and rendering methods used for extracting structural and dynamical information from a given position-time series have been presented in previous sections. We now discuss the design decisions taken while integrating the analysis and rendering tasks to develop the atomistic visualization system.

5.1. Layered structure

Our visualization system is designed in a layered fashion (see below). At the bottom, there are rendering functions to render lines, spheres, cylinders and ellipsoids, and data structures to handle various kinds of data processed in real time. The layers above this provide functionalities for analysis and visualization. The visualization algorithms have direct access to the underlying rendering algorithms and low-level data structures, and also to the analytical algorithms on the same layer.

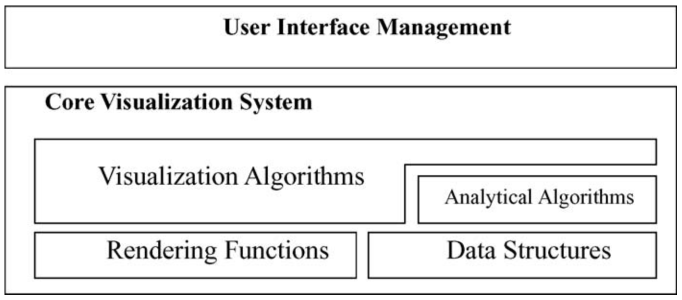

Rendering Functions: Atoms are modelled as spheres and their relationships (bonds and coordination environment) with other atoms are modelled as cylinders and polyhedra. Atomic movements are represented in the form of spheres and ellipsoids. Rendering functions are responsible for setting up material properties of the graphical objects, setting up the lighting parameters and drawing primitives. They are also responsible for setting up the shading context to execute the vertex and fragment shaders. The visualization algorithms frequently make use of these functions to convert information into various graphical forms. Rendering a system containing hundreds of atoms and hundreds more of bonds normally requires transferring massive amounts of polygon information from CPU to GPU. For very large systems, the number of polygons eventually becomes a bottleneck. In polygon based rendering, the quality degrades with the size of the viewport. One way to overcome these problems is to use the

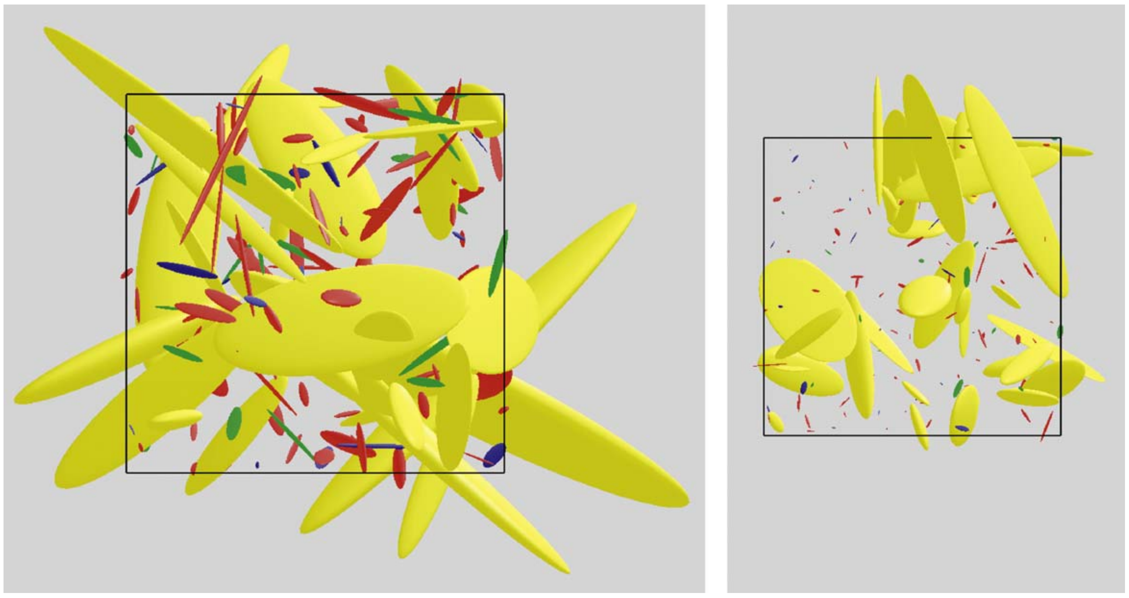

Fig. 18. Ellipsoids representing aggregate motions (over 5 ps) of Mg, Si, O and H atoms in the hydrous silicate liquid at the equilibrium (*left*) and compressed (*right*) volumes at 6000 K. Note that ellipsoids are scaled down from their actual sizes by a factor of 10.

programmability of modern GPU to render quadric objects such as spheres and cylinders. Hardware accelerated algorithm for quadric rendering [35] is implemented as the vertex shader and fragment shader programs. The vertex shader receives the center position of the quadric, size of the quadric, projection matrices and viewport information from the application and computes the size of the point that completely covers the quadric. The fragment shader then computes per pixel normal information and performs lighting computation for each pixel. This results in a high quality output, which is screen-resolution independent (i.e., the quality remains high irrespective of the viewport size) because the algorithm uses implicit function for the rendering.

Data Structures: The individual modules maintain their own data structures to manage the module specific information. This way provides higher-level interfaces to the underlying data that other algorithms can use to provide higher-level functionalities and to reduce the unnecessary recomputation. We present three important data structures: First, the coordination computation time is linearly dependent on the number of time steps. Also the number (s) of species plays a role in the computation time since one needs to deal with a square coordination matrix of order s. A special data structure is designed to enable exploration of various coordination properties without extensive overhead of recomputation. The coordination environments for all pairs of species, α and β, are stored in separate data structures, $ce^{i}_{\alpha\beta}(t_1, t_2, r_1, r_2)$, where $i \in N_\alpha$. The data structure contains complete information about coordination environment for a pair of species including the coordination states, stabilities, distribution and cluster. The contents depend on the range of time steps (t_1 and t_2) and the range of cutoff distances (r_1 and r_2). They are used to compute and render the information in going from one visualization session to another session. Only when either the time or distance range is changed, the contents of the data structure changes and have to be updated. Now, we formally define the data structure:

$$\mathrm{ce}^{i}_{\alpha\beta}(t_1, t_2, r_1, r_2) = (J, D) \tag{18}$$

where

$$\begin{aligned} J &= \{(j \in N_\beta, T) \mid \exists ts.t. r_1 \le d(p_i(t), p_j(t) \le r_2\}, \\ T &= \{t_1 \le t \le t_2 \mid r_1 \le d(p_i(t), p_j(t) \le r_2\} \end{aligned} \tag{19}$$

and

$$D = \{(m, t_m)\}. \tag{20}$$

Here J is the set of pair of atom j of species β that is coordinated with the atom i of species α, at least, once within the selected time range and T is the set of times where the atom i was coordinated with atom j. This set contains the coordination cluster of the atom i. D is the set of pairs of numbers where first element, m, is the coordination number and the second element, t_m, is the total time the atom i had m coordination number. So, D effectively contains the coordination stability information for the atom i. The bond stability between atom i and atom j is given by $|T|/\tau$ for the total selected time range ($\tau = t_2 - t_1$). Note that $|T|$ is the total time the atom i was bonded with atom j given by the corresponding T set in J. We can also calculate the coordination number of atom i for the current time, t, as follows:

$$C^{i}(t) = |\{j | t \in T \text{ where} T \in (ce^{i} \bullet J)_j\}| \tag{21}$$

Here, $(cei{\cdot}J)_j$ is the set J of the atom j.

The common neighbor cluster computation maintains an extensive data structure. The computed CN clusters are stored in a separate data structure so that the clusters can be explored according to different criteria such as the number of common neighbors and the number of bonds between the common neighbors. `ClusterList` holds the information about the number of common neighbors in the cluster. As more than one pair can have the same number of common neighbors, all the clusters having the same number of common neighbors are added to the `ClusterInfoList`, which holds the information about the number of bonds in the cluster among the common neighbors. All the clusters having the same number of bonds among the common neighbors are added to `ClusterInfo`, which contains the detail information about the cluster. It contains the pair of atoms (`startAtom` and `endAtom`), the number of common neighbors between them (`numCommonNeighbors`), the number of bonds among the common neighbors (`numBonds`), the list of common neighbors (`listCN`) and the actual cluster formed by the common neighbors (`cluster`). The `cluster` simply stores the information about the connection among the common neighbors.

If two common neighbors are bonded, then the corresponding entry in the cluster is 'true', otherwise the entry is 'false'.

Finally, the ring structure computation algorithm maintains a shortest distance map apart from the graph data structure to store the shortest distance between selected point and all the other points. The shortest distance maps among all vertices in the graph are computed using Dijkstra's shortest distance algorithm for undirected graphs. The graph is stored in an adjacency list representation for reduced memory consumption. As the rings are computed, the algorithm also maintains the list of currently computed rings.

Analytical Algorithms: The analysis algorithms operate on the data maintained by the data structures to provide a higher-level picture of the underlying dataset. For example, information maintained by the coordination data structure is used to compute coordination stability, coordination cluster, and polyhedral surface among other things. These algorithms have access to the data structures but not have access to the rendering functionalities. Such separation allows for an easy addition of other analytical functionalities in future.

Visualization Algorithms: The visualization algorithms utilize all the other modules to provide an interface to the underlying dataset. They utilize rendering functions to present the information generated by the analytical algorithms. The visualization algorithms also have access to the underlying raw dataset so that the data points can be rendered in their raw form without any extra information attached to them.

User Interface Management: The user interface represents an integrated view of multiple visualization approaches and enables active interaction with the system. It provides options to rotate, translate and scale the scene, to select a group of atoms and analyze relevant attributes of the set of atoms. The user can use the two markers provided in the RDF plot to select the minimum and maximum cutoff distances for any pair of species. Any change in a parameter results immediate visual feedback facilitating visual exploration. Push buttons, selection boxes and textboxes are used to design a prototype user interface. The user interface provides access to underlying analyses and rendering parameters. These parameters control information extraction from the dataset and final graphical output generation. The complete set of the parameters for the currently selected module is readily available from the currently shown interface. There is no need to navigate multiple levels of menu hierarchy to change one parameter. We provide solution to occlusion problem by supporting selective dynamic manipulation scheme, which combines various options such as selective rendering, multiple rendering and transparency [36]. Browsing and highlighting options are added to relate various objects on the scene. The user interface is changed according to which visualization module is selected. The parameter set for the selected module can be changed immediately.

A spreadsheet-like interface is implemented to have a comparative analysis among different outputs in a very primitive form; a more complete interface is supposed to provide the typical features such as a tabular layout, operator and dependency between the cells [37]. The interface makes frequent use of multiple viewports. For instance, if there are s species, the screen will have $s2$ viewports showing coordination between all possible pairs of species. The user can select any particular viewport to further explore the coordination environment in more detail; currently selected viewport is indicated by a red-rectangle around the viewport. It is also possible to select a subset of pairs of species from the set of all pairs of species in the system. Suppose the user selects λ pairs of species from $s2$ pairs of species. Let w and h are the width and height of the window screen on which we want to map λ pairs of coordination environments. If λ is a perfect square, the screen is split along both width and height into $\sqrt{\lambda}$ parts, each with $w/\sqrt{\lambda}$ and $h/\sqrt{\lambda}$. If λ is not a perfect square, the screen is split along both width and height into $\lfloor\sqrt{\lambda}+0.5\rfloor$ parts of $w/\lfloor\sqrt{\lambda}+0.5\rfloor$ and $h/\sqrt{\lambda}+0.5\rfloor$. Then λ selected pairs of species are mapped into λ individual viewports.

5.2. Information representation

Our scheme can be viewed as a special case of hybridization of scientific visualization and information visualization. The atomic position-time series dataset represents a real material system and when the dataset is rendered, the physical relevance (3D atomic arrangement) is to be reproduced/preserved. Each snapshot representation consists of displaying the constituent atoms as spheres of varying color and size according to their species. A periodic table is integrated into the system to make a consistent representation of atomic species across different systems. Subsequent analyses generate additional data that represent information that does not have any direct physical relevance. Such information can be superimposed with the physically relevant data and rendered in a more flexible way. Our system uses color and intensity, size, thickness, shape and geometrical objects to represent various kinds of information extracted during the visualization and analysis process.

5.2.1. Color and intensity

For discrete data like atomic species or coordination numbers, we can use an indexed color map. But for a continuous quantity like time or distance, we design a transfer function, $t(v)$, that assigns a color c according to the value v. For example,

$$c \equiv t(v) = \left[\frac{v}{v_{\max}}, 1 - \frac{v}{v_{\max}}, 0, 1\right] \tag{22}$$

Here, $v_{\max}$ is the maximum value that the quantity can take. The output is in RGBA format. The R and G components vary between 0.0 and 1.0 where as the B and A components always remain fixed. Variation in the bond length, r, of a given bond between $r_{\min}$ and $r_{\max}$ is quantified using

$$\lambda_B = \frac{r - r_{\min}}{r_{\max} - r_{\min}} \tag{23}$$

which varies from 0 (when two atoms are separated by the minimum distance) to 1 (when the atoms are separated by the maximum distance). Now we can define a transfer function like one defined above for $v = \lambda_B$ and also use an index color map by finding the index number as $i = \lfloor \lambda_B i_{\max} \rfloor$.

The intensity of the color depends on the viewpoint so it may not represent the information uniquely. We have used the intensity to encode the stability of the coordination polyhedron for which the color represents the coordination number. This is effective in conveying relative stabilities among different polyhedra within a snapshot or between two snapshots (Fig. 11).

5.2.2. Size and thickness

The size of a sphere in the ball-and-stick representation of coordination encodes the stability of the coordination state (which is represented by the sphere's color) of the central atom. The size is also used to encode the extent of atomic displacement. The thickness of a bond is used to visualize the stability of an atomic bond. A minimum size or thickness is always assigned to make an atom or a bond visible.

5.2.3. Geometric objects

Points, lines, spheres, cylinders, polyhedra and ellipsoids are used. Atoms are usually displayed as spheres but those atoms, which are not the focus in the current snapshot, are drawn as points for the context. The atom trajectories are obtained either by drawing points at the atomic positions as a function of time or by drawing line segments between two successive atomic positions as a function of time. Bonding and coordination relationships between atoms are displayed as lines or cylinders. Polyhedra are used to represent the coordination environment and structural unit. Finally, spheres and ellipsoids are used to represent the atomic movements.

5.3. Information presentation

There is simply too much information to present on the display screen of a finite size. The data points, in our case the atoms, have many attributes; some of the attributes are specified in the dataset and several others are computed on the fly. Different types of information often need to be presented together. Our information presentation scheme exploits the essence of overview, details-on-demand, focus + context, and zoom-and-filter techniques. Animation, pathlines and RDF provide a complete overview of the data. Initially we do not know which temporal region can be of interest and animation gives some idea in this context. The displacement spheres and ellipsoids also provide aggregate information about the system dynamics. Once a temporal interval is selected, one particular atom or a set of atoms can be selected for further exploration. Spatial region around an atom or a group of atoms can be zoomed and explored further using the selective display feature. The RDF provides a complete spatial map of the data. The interpretation of the specific features of RDF requires a detailed structural analysis. The coordination environment and coordination distribution, different types of cluster structures, ring structures, bond-lifetimes, structural stability can be explored on demand for different cutoff distances and cutoff windows. The computed quantitative information can also be saved to files for future analysis by other external tools.

5.4. Programming language and libraries

The C/C++ programming language is used for the system development. The standard template library in C++ provides performance guarantee of the data structures and algorithms in the library. OpenGL (www.opengl.org) is used for graphics rendering supplemented by GLUT and GLUI libraries. OpenGL provides the algorithms for drawing geometric primitives such as points, lines and triangles and defining lighting environment. GLUT library abstracts away the underlying graphics context initialization and management, and presents a cleaner interface useful for application development. GLUI is a user interface library built upon GLUT and OpenGL. We also take advantage of hardware accelerated graphics rendering; a shader program written in GLSL (OpenGL shading language) is executed directly in GPU and is also faster compared to a normal program written in high-level languages executing in CPU. The shader improves the rendering performance and enables highly flexible rendering algorithm to be implemented. Programs written using GLSL are compiled during the runtime and OpenGL drivers come with built-in compiler for GLSL. Qhull [13] algorithm is used to compute coordination polyhedra. It uses the “beneath and beyond” algorithm to compute coordination polyhedra. MATLAB^{TM} C/C++ libraries are used to compute eigenvalues and eigenvectors of the covariance matrices required during the principal component analysis for diffusion ellipsoid.

5.5. Performance

Our visualization system is expected to enable user to explore dataset quickly by providing higher frame rates. We took various optimization measures to ensure that the visualization system is interactive and responsive. A selected subset of the complete positional dataset is stored in the main memory and a separate coordinator module coordinates the access to the dataset. Data structures are constructed dynamically from the positional dataset for different analytical and visualization modules. These modules cache their previously computed results until some parameter is changed avoiding the unnecessary computation. Some analytical algorithms take too long for an interactive visualization. Such intensive algorithms are implemented in separate threads so that they do not deteriorate the interactivity of the system and also do not corrupt the data. Benefit of increased responsiveness outweighs the extra overhead associated with multithreads. Outputs from these algorithms are made available for exploration as soon as new data is computed. As discussed in previous sections, we have adopted various optimization schemes to accelerate RDF, coordination and ring computation. It is shown that the interactive frame rates are achievable for systems consisting of up to a thousand atoms and a couple of hundred thousand time steps in a normal desktop environment. Such system sizes are typical in the case of today’s common first-principles molecular dynamics simulations of a wide range of materials problems including liquids, which are used to justify the effectiveness and usefulness of our atomistic visualization scheme.

6. Conclusions

In this paper, we have proposed an efficient scheme to gain insight into the position-time series data generated by molecular dynamics simulations by going beyond direct rendering of the data. Our scheme integrates various analysis and rendering tasks together in order to support interactive visualization of the data at space–time multiresolution. It starts by processing the original positional data to extract additional data representing information about several relevant structural (radial distribution functions, coordination environments, clusters and rings) and dynamical (diffusion coefficients, atomic displacements and covariance matrices) properties. These data are generated on the fly and rendered interactively at varying levels of details. It is the integration of analytical and rendering methods that makes our study different from the most of the existing visualization systems that are applicable for atomic and molecular systems. While a number of analysis methods have been supported in this study, additional methods can be incorporated as needed. We have achieved the interactive frame rates for systems consisting of up to a thousand atoms and a couple of hundred thousand time steps in a normal desktop environment. Making our visualization system scalable with system size is important since ever larger supercells and longer runs are expected to be amenable to the first-principles MD method in coming days. Although only the FPMD simulation data of moderate size were visualized in this work, one can also visualize the results from pair potentials-based MD simulations of relatively much larger size. Another reason is that a better understanding of the physical system or problem in the question often requires a simultaneous processing of multiple data sets in the same visualization. One feasible approach to addressing the scalability issue is to implementation in multi-processor (parallel) computing and multi-display environments. Besides, faster algorithms for compute-intensive tasks such as ring-analysis algorithm designed for large graphs [31] need to be developed/implemented. Due to the distributed nature of relevant data sources and potential users, it is also desirable to develop support for remote (web-based) atomistic visualization. Finally, the proposed scheme only deals with the visualization of geometric (atomic) structure and dynamics of the simulated systems. The FPMD simulations produce a variety of data related to electronic structures in addition to position-time series. They include electron (charge) distribution, electronic wave functions, density of states, bond overlap populations, etc. Visualization of these data needs to be integrated with the visualization of atomic configurations as was done in a few previous studies, e.g., [3], for instance, superimposing electron density isosurfaces on atomic configurations.

Acknowledgement

This work is supported by National Science Foundation (EAR-0809489 and EAR-0347204).

References

[1] P.J. Kraulis, MOLSCRIPT: A program to produce both detailed and schematic plots of protein structures, Journal of Applied Crystallography 24 (1991) 946–950.
[2] W. Humphrey, A. Dalke, K. Schulten, VMD—Visual molecular dynamics, Journal of Molecular Graphics 14 (1996) 33–38.
[3] A. Kokalj, XCrySDen—a new program for displaying crystalline structures and electron densities, Journal of Molecular Graphics and Modelling 17 (1999) 176–179.
[4] J. Li, Atomeye: an efficient atomistic configuration viewer, Modelling and Simulation in Materials Science and Engineering 11 (2003) 173–177.
[5] A. Sharma, R.K. Kalia, A. Nakano, P. Vashishta, Scalable and portable visualization of large atomistic datasets, Computer Physics Communications 163 (2004) 53–64.
[6] A. Sharma, A. Haas, A. Nakano, R.K. Kalia, P. Vashishta, S. Kodiyalam, P. Miller, W. Zhao, X. Liu, T.J. Campbell, Immersive and interactive exploration of billion-atom systems, Presence 12 (2003) 85–95.
[7] J. Li, Atomistic visualization, in: S. Yip (Ed.), Handbook Materials Modeling, Springer, 2005, pp. 1051–1068.
[8] M.P. Allen, D.J. Tildesley, Computer Simulation of Liquids, Oxford University Press, 1987.
[9] L. Stixrude, M.S.T. Bukowinski, Rings, topology, and the density of tectosilicates, American Mineralogist 75 (1990) 1159–1169.
[10] R.J. Rustad, D.A. Yuen, F.J. Spera, Molecular dynamics of amorphous silica at very high pressures (135 GPa): thermodynamics and extraction of structures through analysis of Voronoi polyhdera, Physical Review B 44 (1991) 2108–2123.
[11] D. Bhattarai, B.B. Karki BB, Visualization of atomistic simulation data for spatio-temporal information. in: WSCG 2006, The 14th International Conference in Central Europe on Computer Graphics, Visualization and Computer Vision (2006) 17–24, ISBN 8086943-03-8.
[12] D. Bhattarai, B.B. Karki, L. Stixrude, Space-time multiresolution atomistic visualization of MgO and $MgSiO_3$ liquid data, Visual Geoscience 11 (2006) 11.
[13] D. Bhattarai, B.B. Karki BB, Atomistic visualization: on-the-fly data extraction and rendering, in: ACM 2007, Proceedings of the 45th Annual Scouthest Regional Conference, ACM (2007) 437–442, ISBN 978-1-59593-629-5.
[14] M. Mookherjee, L. Stixrude, B. Karki, Hydrous silicate melt at high pressure, Nature 452 (2008) 983–986.
[15] D. Faken, H. Jonsson, Systematic analysis of local atomic structure combined with 3D computer graphics, Computational Materials Science 2 (1994) 279–286.
[16] J.P. Rino, I. Ebbsjo, R.K. Kalia, A. Nakano, P. Vashishta, Structure of rings in vitreous SiO_2, Physical Review B 47 (1993) 3053–3062.
[17] B.B. Karki, D. Bhattarai, L. Stixrude, First-principles calculations of the structural, dynamical, and electronic properties of liquid MgO, Physical Review B 73 (2006) 174208.
[18] P. Hohenberg, W. Kohn, Inhomogeneous electron gas, Physical Review 136 (1964) B864–B871;
W. Kohn, L.L. Sham, Self-consistent equations including exchange and correlation effects, Physical Review 140 (1965) A1133–A1138.
[19] B.B. Karki, D. Bhattarai, L. Stixrude, First-principles simulations of liquid silica: Structural and dynamical behavior at high pressure, Physical Review B 76 (2007) 104205.
[20] C.B. Barber, D.P. Dobkin, H. Huhdanpaa, The quickhull algorithm for convex hulls, ACM Transactions on Mathematical Software 22 (1996) 15.
[21] K. Robinson, G.V. Gibbs, P.H. Ribbe, Quadratic elongation—quantitative measure of distribution in coordination polyhedra, Science 171 (1971) 567–570.
[22] N.W. Thomas, Crystal structure-physical property relationships in perovskites, Acta Crystallography B45 (1989) 337–344.
[23] E. Blaisten-Barojas, Structural effects of three-body interactions on atomic micro-clusters, Kinam 6A (1984) 71.
[24] J.D. Honeycutt, H.C. Andersen, Molecular dynamics study of melting and freezing of small Lennard-Jones clusters, Journal of Physical Chemistry 91 (1987) 4950–4963.
[25] H. Tsuzuki, P.S. Branicio, J.P. Rino, Structural characterization of deformed crystals by analysis of common atomic neighborhood, Computer Physics Communications 177 (2007) 518–523.
[26] A. Jain, V. Kumar, Y. Kawazoe, Ring structures of small ZnO clusters, Computational Materials Science 36 (2006) 5.
[27] M.R. Sahar, A.W.M.A. Hussein, R. Hussin, Structural characteristic of Na_2O–P_2O_5–GeO_2 glass systems, Journal of Non-Crystalline Solids (2007).
[28] S.V. King, Ring configurations in a random network model of vitreous silica, Nature 213 (1967) 1112–1113.
[29] J.B. Hendrickson, D.L. Grier, A.G. Toczko, Condensed structure identification and ring perception, Journal of Chemical Information and Computer Sciences 24 (1984) 193–195.
[30] X. Yuan, A.N. Cormack, Efficient algorithm for primitive ring statistics in topological networks, Computational Materials Science 24 (2002) 18.
[31] C. Zhang, B. Bansal, P.S. Branicio, R.K. Kalia, A. Nakano, A. Shrama, P. Vashishta, Collision-free spatial hash functions for structural analysis of billion-vertex chemical bond networks, Computer Physics Communication 175 (2006) 339–347.
[32] J. Rybicki, G. Bergmanski, G. Mancini, A new program package for investigation of medium-range order in computer-simulated solids, Journal of Non-Crystalline Solids 293–295 (2001) 758–763.
[33] K. Goetzke, H.-J. Klein, Properties, efficient algorithmic determination of different classes of rings in finite and infinite polyhedral networks, Journal of Non-Crystalline Solids 127 (1991) 215–220.
[34] I.T. Jolliffe, Principal Component Analysis, Springer-Verlag, 1986.
[35] C. Sigg, et al., GPU-based ray-casting of quadratic surfaces, in: Eurographics Symposium on Point-Based graphics, The Eurographics Association, 2006.
[36] C. Everett, Interactive order-independent transparency. Technical Report, NVIDIA Corp., 2001. (http://developer.nvidia.com/).
[37] E.H.-h. Chi, et al., Principles for information visualization spreadsheets, IEEE Computer Graphics and Applications 18 (1998) 30–38.